To the Graduate Council:

I am submitting herewith a thesis written by Michael L. Languell entitled "Correlation of Surface Finish and Cover Gas with Weld Defects in Autogenous Al 5083 Laser Beam Welds." I have examined the final copy of this thesis for form and content and recommend that it be accepted in partial fulfillment of the requirements for the degree of Master of Science with a major in Engineering Science and Mechanics.

Mary Helen McCay

Mary Helen McCay, Major Professor

We have read this thesis
and recommend its acceptance:

Reinhard Menzel

J Dwayne McCay

Monty Smith

Accepted for the Council:

Lew Winkel

Vice Provost
and Dean of The Graduate School

STATEMENT OF PERMISSION TO USE

In presenting this thesis in partial fulfillment of the requirements for a Master's degree at the University of Tennessee, Knoxville, I agree that the Library shall make it available to borrowers under the rules of the Library. Brief quotations from this thesis are allowable without special permission, provided that accurate acknowledgement of the source is made.

Permission for extensive quotation from or reproduction of this thesis may be granted by my major professor, or in her absence, by the Head of Interlibrary Services when, in the opinion of either, the proposed use of the material is for scholarly purposes. Any copying or use of the material in this thesis for financial gain shall not be allowed without my written permission.

Signature Michael Langsdell

Date Nov. 30, 1998

CORRELATION OF SURFACE FINISH AND COVER GAS WITH WELD DEFECTS IN AUTOGENOUS AL 5083 LASER BEAM WELDS

A Thesis

Presented for the

Master of Science

Degree

The University of Tennessee, Knoxville

Michael L. Languell

December 1990

ACKNOWLEDGEMENTS

In the course of thesis research, a number of scholars have assisted me generously. In particular I am indebted to Professors Mary Helen McCay, T. Dwayne McCay, Reinhard Menzel, and L. Montgomery Smith, who served as my chairperson and committee respectively. With their diligent guidance, criticism, and encouragement, I was able to achieve experimental and personal results otherwise impossible.

I would also like to thank Drs. C. Parigger and A. Sedghi-Nasab for their invaluable assistance with computer programming, optics, and electronics. No acknowledgements would have been possible without the vast experience with CO_2 lasers of C. Michael Sharp. Also the help supplied by Mike Womack with the Kiethly temperature acquisition system was greatly appreciated. And a big thank you to Leslie Culver and Michelle Parigger for their time proof-reading this manuscript.

ABSTRACT

Aluminum laser weld quality is influenced by gas porosity and surface reflectivity. The experimental study was performed on Al 5083 in three parts: the first, to correlate surface finish and cover gas with porosity formation, the second, to establish the effects of the laser sustained plasma on porosity formation, and the third, to ascertain the effect of surface finish on reflectivity of 10.6 μm radiation at room temperature.

The first part consisted of a series of CO_2 laser welds varying cover gas and surface finish. The subsequent metallographic examination revealed no correlation between surface finish and porosity, but that the cover gas selection strongly influenced the type and quantity of pores formed.

In the second part, laser welds were made varying only the cover gas while monitoring the spectral emission of the laser sustained plasma. The subsequent gravimetric measurement of porosity and the emitted spectrum from the plasma indicated a linear relationship between hydrogen content of the plasma and the quantity of porosity.

Calorimetric measurements of the absorptivity were made on the surface treatments of the first part. The reflectivities inferred from these measurements were 97%, 94%, 26.6%, and 78.3% for the polished, brushed, blackened, and sandblasted surfaces, respectively.

TABLE OF CONTENTS

CHAPTER		PAGE
I.	INTRODUCTION	1
II.	BACKGROUND	5
III.	EXPERIMENTAL	18
IV.	RESULTS	29
V.	DISCUSSION	32
VI.	CONCLUSIONS	37
LIST OF REFERENCES		39
APPENDIXES		42
	APPENDIX A	43
	APPENDIX B	45
VITA		80

LIST OF TABLES

TABLE PAGE

II-1. Composition Al 5083..... 46

II-2. Properties Al 5083..... 46

III-1. Study Matrix (Part A)..... 47

III-2. Study Matrix (Part B)..... 47

III-3. Weld Parameters (Parts A & B)..... 47

III-4. Gas Properties..... 48

IV-1. Average weld depths, widths and areas (Part A).... 49

IV-2. Results (Part B)..... 50

LIST OF FIGURES

FIGURE		PAGE
II-1.	Depth to Width Ratio	51
III-1.	Schematic drawing of instrument set-up	52
III-2.	Schematic drawing of optical table	53
III-3.	Schematic drawing of experimental arrangement for the thermal absorption runs with a detail of the sample	54
III-4.	Schematic drawing of Al 5083 sample with surface treatments	55
III-5.	Scanning electron micrographs of Al 5083 surface finishes (300X)	56
III-6.	Sample horizontal intensity data illustrating plasma width determination	57
IV-1.	Averaged depth to width ratios from 'A' runs grouped by surface treatment. (Bars indicate maximum and minimum values)	58
IV-2.	Averaged depth to width ratios from 'A' runs grouped by cover gas. (Bars indicate maximum and minimum values)	59
IV-3.	Example of type 1 and type 2 porosity	60
IV-4.	Example of type 3 and type 4 porosity	61
IV-5.	Average pores per square mm from 'A' runs grouped by surface finish	62

FIGURE PAGE

IV-6. Average pores per square mm from 'A' runs grouped by cover gas..... 63

IV-7. Laser induced plasma over polished Al 5083 for various gases..... 64

IV-8. Laser induced plasma over brushed Al 5083 for various gases..... 65

IV-9. Laser induced plasma over blackened Al 5083 for various gases..... 66

IV-10. Laser induced plasma over sandblasted Al 5083 for various gases..... 67

IV-11. Averaged spectrum of plasma with He 5% H_2.....68

IV-12. Averaged spectrum of plasma with argon..... 69

IV-13. Averaged spectrum of plasma with helium..... 70

IV-14. Averaged spectrum of plasma with wet helium..... 71

IV-15. Averaged spectrum of plasma with wet argon..... 72

IV-16. Averaged spectrum of plasma with wet He 5% H_2....73

IV-17. Thermal history for surface absorptivity run on polished surface..... 74

IV-18. Thermal history for surface absorptivity run on brushed surface..... 75

IV-19. Thermal history for surface absorptivity run on blackened surface..... 76

IV-20. Thermal history for surface absorptivity run on sandblasted surface..... 77

FIGURE PAGE

V-1. Plot of normalized area under H_α peak versus percent porosity for helium-based cover gases (Normalized to helium)..... 78

V-2. Plot of normalized area under H_α peak versus percent porosity for argon-based cover gases (Normalized to argon)..... 79

CHAPTER I

INTRODUCTION

The efficient joining of components is of paramount importance to many industries. For numerous applications, welding is the best method for joining similar or even dissimilar metals. This study is an experimental investigation of porosity formation in aluminum alloy 5083 for laser welding. The approach is to study the effects of surface finish and cover gas on porosity formation and relate how the aspects of laser beam welding (LBW) affect porosity.

The quality of a weld is defined in terms of the absence of weld discontinuities. A weld discontinuity is an undesirable deviation in the physical structure of a welded component. Weld discontinuities may be classified as design related, process related, or metallurgical. Design related discontinuities are primarily due to the improper selection of the weld joint or structure. Process related discontinuities include: porosity, shrinkage voids, oxide inclusions, lack of fusion (LOF), lack of penetration (LOP), and craters. Porosity is cavity-like discontinuities formed by gas entrapment during solidification. Other metallurgical discontinuities include: cracks, fissures, segregation, and lamellar tearing.[1]

The alloy selected was Al 5083, an aluminum - magnesium alloy that has important applications in the automotive, marine and aerospace industries. However, due to welding difficulties its use has been restricted.[2] These welding difficulties include: distortion, high residual stress, and high porosity. Another sensitive area in regard to the welding of Al 5083 is the potential loss of magnesium, which is the source of the desirable high strength properties of Al 5083.

Laser beam welding (LBW) was selected for this study due to its production advantages over conventional welding processes. These advantages include:

1) No electrode, hence no contamination from electrode, and more consistent heat input.
2) High energy density leading to localized heating and rapid cooling, minimizing the heat affected zone, and lowering distortion.
3) Laser beams can be optically manipulated to otherwise inaccessible areas during fabrication.

The present knowledge in the area of LBW weld discontinuities in aluminum alloys is incomplete.[3] Surface finish of the workpiece was rarely reported in the LBW papers in the open literature.[4]

The objectives of the study were to qualify the effects of surface finish and cover gas on process related weld discontinuities, and to establish the relationship between

porosity formation and the laser induced plasma during LBW of Al 5083. Two series of autogenous (without filler metal) laser beam welds were performed. The first series (Part A) of laser welds was done with different surface treatments and cover gases while recording the plasma image on standard television video tape. The second series (Part B) of laser welds was performed on a brushed surface with different cover gases while monitoring the spectral emission and intensity of the plasma. A third experiment (Part C) was performed to determine the effect of the surface treatments used in part A on the reflectivity of solid Al 5083.

A metallurgical characterization of the weld bead was made following the first series (A). The characterization included sectioning, polishing, etching and optically examining the weld. The porosity (total) was determined with gravimetric measurements and radiography following the second series (B) of laser welds. The absorptance of incident radiation was found in part C by using calorimetric measurements from which an estimate of the reflectivity was established. The work for this study was accomplished at the Center for Laser Applications, University of Tennessee Space Institute, Tullahoma, Tennessee.

The background chapter provides a description of porosity formation in conventional and laser aluminum welds

along with a survey of the current literature on the subject. The experimental chapter describes the equipment, procedures, and data analysis used to perform the necessary work. The results chapter presents the experimental data. The discussion chapter includes the interpretation of the results.

CHAPTER II

BACKGROUND

A. Conventional Welding

Welding is the joining of two or more pieces of metal by applying heat or pressure, or both, with or without the addition of filler metal, to produce a localized union through fusion or recrystalization across the interface.[5] Conventional welding methods for aluminum are Gas Metal Arc Welding (GMAW) and Gas Tungsten Arc Welding (GTAW).

GMAW is a welding process in which heat is generated by an electrical arc between a consumable electrode and the workpiece.[6] The consumable electrode becomes the filler metal as it is continuously fed into the weld area. A shield gas is fed to the weld area through the welding gun and is used to shield the electrode, weld pool and the adjacent base metal. The shield gas is of extreme importance because even a small amount of atmospheric air will have deleterious effects on the properties of the resulting weld. The advantages of the GMAW process are high productivity, reliability, all-position welding capability, ease of use, and low cost. The disadvantages of GMAW include consumable electrode, conduction-limited penetration, and a power supply needed at each work station.

GTAW is a welding process in which the heat for welding is generated by an electrical arc between a non-consumable tungsten electrode and the workpiece.[7] A shield gas is needed as in GMAW for the same reasons. The electrode is non-consumable; thus, a weld can be made without the addition of a filler metal depending on the requirements of the joint. GTAW is best suited for the welding of thin metal (1/8 inch).[7] The advantages of GTAW include the ability to weld most metals, even those that form refractory oxides like aluminum and magnesium, all-position welding, and filler metal is not always required. The disadvantages of GTAW include slow welding speed, the requirement for highly skilled operators, contamination of the electrode, and particles from the tungsten electrode entering the weld pool.

The typical problems associated with conventional welding methods of aluminum are distortion, LOF/LOP, and porosity. Distortion is a result of excessive heat input which is needed to produce welds of sufficient depth in materials of high thermal conductivity, i.e. aluminum and its alloys. If insufficient heat is input to the weld or the input heat does not reach the weld pool, then LOF or LOP will result.

The depth to width ratio, defined in Figure II-1, is often used as an indication of deep penetration welding as compared to conduction-limited welding. The factors that

affect weld penetration are the welding techniques, thermal properties of the base metal, and surface contaminants.[8] Welding techniques that result in lack of penetration are low amperage, over-sized electrode, and high weld speeds; all of these cause insufficient delivery of heat to the weld pool. High levels of surface contaminants will prevent the heat of the arc from reaching the underlying metal. A weld on a base metal with a high thermal conductivity (such as aluminum) will tend to be broad because the heat input to the weld surface is rapidly conducted into the surrounding workpiece resulting in a low depth to width ratio.

Hydrogen gas is the primary source of porosity in aluminum welds[9] because mere trace levels (120 ppm)[10] of hydrogen in the arc will result in porosity in the weld. Sources of hydrogen in welds are hydrocarbons and moisture on and in the base and filler metals, and atmospheric humidity. The hydrocarbons and moisture are converted to atomic hydrogen by the arc and is subsequently transferred to the weld pool.

During solidification of aluminum alloy welds, hydrogen in the melt is rejected at the liquid-solid interface in much the same manner as solute is rejected in alloys having a partition ratio, K, less than unity. The partition ratio is the ratio of the equilibrium solute concentration in the solid to the equilibrium solute concentration in the

liquid. The equilibrium concentration of hydrogen in solid aluminum at the solid-liquid interface is $3x10^{-6}$ weight percent.[11] The equilibrium concentration of hydrogen in liquid aluminum at the solid-liquid interface is $6x10^{-5}$ weight percent.[11] The partition ratio for hydrogen in aluminum is then 0.05.[11] During solidification, if the concentration of hydrogen in the liquid is less than the maximum solubility of hydrogen in solid aluminum ($3x10^{-6}$ weight percent) at the freezing temperature, then bubbles will not form and the resultant weld will be pore free. When the hydrogen concentration in the liquid exceeds the maximum solid solubility at the solidus temperature, the excess hydrogen is rejected into the liquid. If the solubility of hydrogen in liquid aluminum ($6x10^{-5}$ weight percent) is exceeded, bubbles are nucleated which can then be frozen into the weld resulting in porosity. Primary porosity results from hydrogen bubbles forming in the liquid, and secondary porosity results from hydrogen precipitating from the solid.

Primary porosity exhibits two morphologies, spherical and interdendritic.[12] Spherical porosity is observed in highly supersaturated liquids and is surface tension dependent. The interdendritic variety of primary porosity is observed when the weld pool is at low to moderate levels of supersaturation with hydrogen and is growth-substructure dependent. The size, shape, and growth rate

of the interdendritic porosity depends on the solidification mechanisms of the specific aluminum alloy. GMAW and GTAW usually produce cellular-dendritic structure in aluminum welds. The nucleated bubbles can grow between the cellular-dendrites, but cannot escape and flow into the weld pool at moderate growth rates. If the bubble is small and entrapped between the cellular arms, its high surface tension will tend to maintain a spherical shape. Large interdendritic bubbles have a greater tendency to escape entrapment due to buoyancy forces. However, should a large bubble become entrapped, a non-spherical pore is more likely to be produced since the surface tension force of the bubble cannot compensate the force of the laterally converging dendrite arms.[12] The entrapment of hydrogen bubbles leading to pores in the weld are dependent upon the solidification morphology, cooling rate, degree of convective flow, welding parameters, shielding gas, and external pressure.[11]

Studies have been performed on the effects of hydrogen on porosity formation in the welding of aluminum.[9,13,14] Martukanitz and Michnuk varied the levels of hydrogen in the cover gas, base, and filler metals while performing GMAW welds on Al 5083 and Al 6061. To obtain low levels of hydrogen content the following were employed: high purity grade argon cover gas, standard filler metal electrodes, and chemically cleaned base metal after dry groove-

machining. High hydrogen content values were obtained with: custom-mixed argon with 0.12% hydrogen, specially fabricated contaminated electrode, and base plate groove-machined with lubricant. They found that the base metal and surface contamination had little effect on porosity and that the porosity was a function of hydrogen levels in the filler metal and cover gas.[9]

The effect of varying the hydrogen (H_2) content in a cover gas of 75% argon - 25% helium while GMA and GTA welding aluminum alloys was studied by R. A. Woods. He found that weld porosity was a function of arc hydrogen content, arc current, arc length, and weld pool surface area.[13]

In Z. P. Saperstien's et al. study of porosity in aluminum welds the test plates were brushed using a stainless steel brush and cleaned with acetone.[14] The test variables were gas preflow, arc voltage, arc current, and cover gas composition. To obtain porosity, the cover gas was contaminated with moisture by bubbling it through room temperature water and by additions of hydrogen (H_2). The same relation of increased porosity with hydrogen content was found with both moisture and hydrogen (H_2) additions to the cover gas.[14]

B. Physics of Laser Welding

LASER is an acronym for Light Amplification by Stimulated Emission of Radiation. A unique aspect of using

a laser as an energy source is that the emitted energy is over a narrow wavelength range. The characteristic wavelength for a CO_2 laser is 10.6 μm.

The development of multikilowatt CO_2 lasers has led to the increased applicability of lasers for welding processes.[15] However, due to the highly reflective nature of most polished metals to 10.6 μm (reflectance > 85%), the desirability of using a CO_2 laser is lessened. Fortunately, the reflectivity is significantly affected by the surface condition.[16]

A laser weld may either be conduction limited or deep penetration depending on the incident power density and the workpiece material. A small depth to width ratio (<<1.0) is characteristic of a conduction limited weld because the heat transfer is by conduction only. In deep penetration welding, the power density is sufficient to cause vaporization of the target material on the weld pool surface. The vaporization of the weld pool creates a cavity in the molten metal. The cavity allows the laser beam to penetrate further into the workpiece, vaporizing more material. The vaporizing and penetrating process continues until the forces (e.g. gravitation and surface tension) tending to close the cavity balance the metal vapor pressure forces to create what is known as the 'keyhole'.[17] When the keyhole is formed, the laser is then 'coupled' to the workpiece via the walls of the keyhole.

The coupling is a result of both the plasma, whose absorptivity and reradiation of the laser radiation is strong[18], and the keyhole, which acts as a blackbody absorber.[19] The effect of the coupling is an increase in efficiency of incident energy absorption to the weld. As the workpiece is translated, the keyhole moves with the laser beam. The molten metal in front of the keyhole flows around the sides of the cavity and solidifies to the rear, forming the weld bead.[20]

Now that the basic physics of laser welding has been reviewed, each aspect of the process will be discussed in relation with hydrogen porosity formation compared to conventional welding. Namely, the effects of the plasma, keyhole, and surface condition on the mechanisms of hydrogen bubble formation and entrapment will be reviewed.

The laser induced plasma is a highly energetic ionic cloud, whose production and properties are strongly influenced by the cover gas and the material properties of the workpiece.[21] The laser induced plasma plays the same role as the arc in conventional welding in the dissociation of moisture and hydrocarbons due to the highly energetic character of the plasma. Since the plasma and the arc are in contact with the weld pool,[22] they can transfer atomic hydrogen to the molten metal.

Besides dissociating moisture and hydrocarbons, the laser induced plasma vaporizes a portion of the weld pool.

It then absorbs incident laser radiation, which the plasma subsequently reradiates. The reradiated energy contains spectral information depending on the constituents of the plasma.

The spectral emission from the laser induced plasma has been investigated[4] and was used to determine the average temperature and constituent elements of the plasma. The technique used to analyze the plasma was as follows. A six millimeter volume above the workpiece was focused onto the entrence slit of a 0.25 meter spectrometer. The transfer optics reduced the plasma image to one millimeter at the plane of the entrance slit. A grating was chosen such that a spectral window of 370 to 430 nanometers was obtained. An optical multichannel analyzer (OMA) recorded 40 spectra during welding with an integration time of 20 milliseconds for each spectra. The relative amounts of the constituent elements in the plasma were found by integrating the area under the line profile. The ratio of two neutral line emission coefficients were used to determine the temperature.

The keyhole produced in deep penetration welding has two effects on the production and entrapment of hydrogen bubbles. The keyhole will result in higher temperatures in the molten metal at the bottom of the weld by delivering incident energy deep into the weld. The increased temperature of the molten metal will increase its hydrogen

solubility, thus increasing the chances of hydrogen bubble formation during solidification. The keyhole translation through the weld pool results in a vortex in the trailing molten metal.[24] The vortex is then an added convective influence not present in conventional welding. Since the entrapment of hydrogen bubbles is affected by the convective flow, an increase in flow would facilitate the escape of hydrogen bubbles from the weld pool. The molten metal flow rates for conventional and laser welding are 0.2 and 1.0 meters per second respectively.[25]

The effects of surface condition in conventional welding were not significant.[9] However, in laser welding of metals the absorption of the incident energy is affected by the surface reflection characteristics. For example, the absorptance of aluminum, at melting temperature, went from 15% to 42% when the polished surface was roughened with sandpaper.[26] The amount of the incident energy absorbed will dictate the solidification morphology. And, as in conventional welding, the solidification morphology will influence the entrapment of hydrogen bubbles.

Arata investigated the effect of surface condition on the absorptance of 10.6 μm radiation on aluminum and stainless steel.[26] The surface treatments on polished metal were: roughened, coated with non-metallic thin film, coated with metallic powder, and irradiation of focused laser beam. The absorptance of the incident 10.6 μm

radiation was found using a calorimeter from which the reflectivity was estimated.[26] Arata performed the absorption experiments in two temperature regimes, at room temperature and at the melting temperature for the given material. The samples for both temperature measurements were 0.3 mm thick.

For the room temperature measurements, Arata used a water-cooled power meter for determining the amount of absorbed energy. Water was flowed through the power meter at a constant rate which was measured by a flow meter, while the inlet and outlet water temperatures were monitored with thermisters. To calibrate the system, a heated was incorporated in the inlet with an electrical input of known power level. The sample was irradiated with an unfocused laser beam of approximately 200 watts on one side while water cooled on the back side.[26]

For the melting temperature measurements, a molten pool was produced by laser heating with a focused beam. Each sample, upon melting, was immediately thrown into a calorimeter and the calorimetric gain was measured. The calorimetric gain was determined by monitoring the temperature rise of the water in the calorimeter with a thermister.

Arata's investigation found, for aluminum, that the surface treatments of coating with a material of lower melting point had the most effect on the absorptance.[27]

C. Rationale for experimental conditions

Since the referenced[9,13,14] studies found that the role of the cover gas dominated in autogenous welds, variation of hydrogen content in the cover gas was employed to study porosity formation in the aluminum laser welding of this study. The resultant porosity was measured using cross section analysis, gravimetric, and radiography techniques used in the referenced[9,13,14] studies.

Arata's findings on the role of surface treatments in laser welding indicates their importance and thus indicates that surface treatments could affect porosity formation in laser welding of aluminum. The surface treatments chosen for this study were a polish (reference), two roughening treatments (brushed and sandblasted) and a non-metallic coating (blackened), to limit the size of the study matrix.

Spectral emission detection from the laser induced plasma can be used to determine the constituents of the plasma; thus for part B, this technique was used to determine the relative amounts of atomic hydrogen present in the plasma.

Al 5083 was selected for this study because of its important industrial applications, welding difficulties, and principle alloying element addition (magnesium). The low ionization potential of magnesium (7.65 eV) and its low vaporization temperature (1380 K) are significant in laser welding due to their facilitating the formation and

sustentation of the laser induced plasma. Noteworthy is the fact that Al 5083 was used in two of the three conventional welding studies on porosity mentioned, thus the results from this experiment can be directly compared with previous work. The composition of Al 5083 is listed in Table II-1 and its material properties are in Table II-2.

CHAPTER III

EXPERIMENTAL

A. Outline

The experimental work for this project was performed in two parts. The first part (A) was to determine the effects of surface condition and cover gas during laser welding of Al 5083 on the porosity and depth to width ratio. Four different surface treatments were used together with five different cover gases. The surface treatments selected were: (1) polished, (2) brushed, (3) sandblasted, and (4) brushed and blackened with carbon soot. The cover gases selected were: instrument air, argon, wet argon, helium, and a mixture of helium with 5% (by volume) hydrogen. During the laser weld runs, video recording of the plasma images was made. A post-process characterization of the weld's cross-section was made to determine the resultant porosity and depth to width ratio. The study matrix of part A weld runs is in Table III-1.

Part B of the project was to determine the atomic hydrogen content and size of the plasma over the weld pool and their relationship to porosity while laser welding Al 5083. The relative hydrogen content of the plasma was found from the spectral data taken with a spectrometer and an optical multichannel analyzer (OMA). A second OMA with a horizontal slit took intensity of the plasma image that

was used to determine the plasma size. Figure III-1 is a schematic drawing of the arrangement of the above-mentioned equipment. Only the brushed surface treatment with different cover gases were employed during the laser weld B runs. The cover gases selected were: argon, helium, and helium with 5% hydrogen in the dry (as-received) and wet states. The study matrix of part B is in Table III-2.

All laser weld runs performed for this project were autogenous bead-on-plate welds. The weld process parameters were held constant, except surface condition and cover gas, and are listed in Table III-3.

To establish the effect of the surface treatments in part A on reflectivity, the absorptance of a defocused incident beam on surface treated samples was found calorimetrically. The reflectivity was inferred from the absorptivity since the radiation, convection, and conduction heat losses from the sample were assumed neglible. Thus a measure of the reflectivity for each of the surface treatments, at room temperature, were found. This method is similar to that used by Arata in that the aborbed energy in determined from a temperature rise.

The primary difference between Arata's method and the one employed in this project for determining the absorptance at room temperature is sample temperature. In Arata's work, the temperature of irradiated sample was maintained at room by using a thin sample and cooling it

with water. Thus, the room temperature absorptance was found indirectly by measuring the rise in the temperature of the water while assuming that all of the energy input to the sample was transfered to the cooling water. Whereas in this project, the energy absorbed by the sample was measured by monitoring the temperature rise in the sample directly. Even though absorptance is a function of temperature, the error introduced by the changing sample temperature was neglible because the temperature rise was not significant.

Equipment Description

A Rofin-Sinar (RS) 3000 RF excited fast axial flow industrial CO_2 laser was used to autogenously bead-on-plate weld Al 5083 alloy. This laser system can be operated in two wave (CW) modes, full power continuous mode or modulated CW mode. The modulated CW mode is pulse modulated at 5 kHz with the duty cycle adjusted to achieve the desired power level. A computer numerical controlled (CNC) workstation was used to control the cover gas flow, laser operation, and the translation of the workpiece during welding.

The video data was taken with a lens system, a solid state Charge Injected Device (CID) surveillance camera and a VHS professional tape recorder. The lens system consisted of a close-up lens on a variable focus lens, and a neutral density filter, chosen with ND=3.5 to prevent the

saturation of the camera. The recording rate was set by the speed of the VHS tape recorder at 30 frames per second. The video data were images of the laser induced plasma during welding and indicated the size and shape of the plasma.

The optical system used in part B to image the plasma on the two OMAs were mounted on an in-house manufactured adjustable optical table (Figures III-1 and III-2). The image focusing was done with a Cassegrain telescope. The plasma image was distributed to the OMAs by using two quartz flats as beam splitters. Two neutral density filters were also included in the system to prevent detector saturation and damage.

The spectrometer in #1 OMA system was calibrated using the locations of lines from a neon low pressure discharge lamp and an argon low pressure discharge lamp. The spectral line corresponding to the energy difference between the first and second excited levels of atomic hydrogen is designated as H_α. The location of the H_α peak was confirmed to lie at the approximate center of the spectral window, 6200 - 7200 Ångstroms, using a hydrogen low pressure discharge lamp. The #2 OMA system was calibrated using a 3 mm slit at the weld pool location illuminated from behind with a bright light source. Both of the OMAs were operated with a sampling interval of 0.02 seconds and collected 50 scans for a total of 25 mm of weld transversed. The spectral (OMA #1) and the horizontal

intensity (OMA #2) data were stored on floppy disk after each laser run.

The temperature of the sample and room were monitored using K-type thermocouples. The sample thermocouple was located at the geometric center of the sample.(Figure III-3 Sample Detail) The room thermocouple was located approximately one foot from the sample and not in contact with any surface. The thermal histories of the sample and the room were acquired and stored on a PC computer with a Kiethly data acquisition and control system. The sample was insulated on the sides and bottom to reduce conduction losses. A schematic drawing of the arrangement of the equipment and sample is given in Figure III-3.

C.Procedures

C-1 All Laser Runs

Prior to the laser weld runs, the cover gas supply lines were purged with the gas to be used. The flow rate was set at 15 scale units. The actual flow rates in liters per minute for air, argon, helium and helium plus 5% hydrogen were 4.1, 3.45, 11.0, and 11.9 respectively. Table III-4 contains the properties of the cover gases employed.

C-2 Sample Preparation

Samples were cut from 0.25 inch-thick stock into 1 x 4 inch rectangular pieces and numbered one through five. The surface treatments were: polishing, brushing, brushing and

blackening with carbon soot, and sandblasting with glass frit. The samples were weighed, measured, and checked for flatness after each surface treatment. The treatments were performed less than an hour prior to welding to ensure consistency and effective removal of impurity surface layers. The final step of each of the treatments was a thorough cleaning with acetone, and drying to remove foreign substances. Figure III-4 is a schematic drawing of a typical sample. Figure III-5 contains scanning electron micrographs (300X) of the surface finishes.

Polishing was completed in two steps. The first step was made with 600 grit emery paper, the second step was made with felt cloth and diamond paste. The brushing treatment consisted of roughing the surface with a stainless steel brush. The treatment of brushing and blackening has the same roughing and cleaning procedure as brushing, but also involves the coating of the surface with carbon soot. Coating the surface with carbon soot was performed using an acetylene and oxygen cutting torch with a rich mixture of gases. Sandblasting was done with an air compressor and fine glass grit.

The sample for the absorption measurements was prepared from the same 0.25 inch thick Al 5083 stock as the weld samples. The sample was machined into a one inch in diameter disk. A hole was drilled in the sample for the thermocouple to the geometric center of the disk. Figure

III-3 includes a detail of the sample. The surface of the sample was prepared using the same techniques as the weld samples for part A.

C-3 Surface Absorption Runs

The laser beam was defocused such that the beam spot was slightly smaller than the sample surface. The sample was then centered under the beam. The sample was irradiated for eight seconds at an indicated power of 500 watts while its thermal history was recorded. The thermal history included seven seconds prior to irradiation, the eight seconds of irradiation and seven seconds following irradiation. After each run the sample was allowed to cool to room temperature. Each surface treatment was irradiated twice to ensure repeatability. The same sample was used, but with different surface finishes, for all of the runs so that the same thermal mass was employed each time.

D. Data Reduction

D-1 Metallurgical Characterization (Part A)

The four surface weld sections were then cut from the parent sample with a band saw. The weld sections were approximately 25 mm in length. Four cross-sections cut from the last 10 mm of the weld were mounted, polished, and etched using standard metallographic techniques. Microphotographs of each cross section were taken and the weld depth, weld width, and weld porosity type and quantity were measured from these microphotographs with a

ruler and knowledge of the magnification. The remaining portion of the welds were sectioned longitudinally along the centerline, polished, etched and photographed using a digital image processing system.

D-2 Video (Part A)

The video data was analyzed using a digital image processing system. A field-by-field review of each image was performed, and representative photographs of the plasmas for each surface finish and cover gas were taken.

D-3 OMA #1 (Part B)

Each of the 50 scans of the spectral data containing the H_α line of hydrogen were averaged together and the average spectrum was plotted versus wavelength. The spectral data was then inspected to find the ranges of adjacent continua to the H_α peak which were used to find the equation of a linear line. The area under the H_α peak for each of the 50 scans was then individually calculated by summing the difference between the data and equation of the linear line. The areas from the 50 scans were averaged and the standard deviation was calculated. The averaged area under the H_α peak for each cover gas was used as a measure of the relative amount of atomic hydrogen contained in the plasma for the given cover gas.

D-4 OMA 2 (Part B)

The 50 scans of second OMA's horizontal intensity data were averaged to obtain a plot of plasma intensity versus

location.(The plasma location remains constant since the workpiece is translated under the laser beam.) The averaged intensity data was normalized and plotted versus location. Figure III-6 is a typical plot. The average width of the plasma at the workpiece was determined by the following methodology. Straight lines were extrapolated from the normalized intensity where the intensity was less than 0.1 on either side of the plasma (A and B)(see Figure III-4). Straight lines were extrapolated from the two 3/4 and 1/4 of maximum intensity points (C and D). The intersections of lines A,C and B,D were taken to be the edges of the plasma.

D-5 Radiography (Part B)

Radiographic plates taken of the welds were developed and the black and white prints were enlarged to facilitate the estimation of porosity. The porosity estimation was used to check the porosity found in the gravimetric measurements.

D-6 Gravimetric (Part B)

Gravimetric measurements were performed on part B welds to ascertain the percentage porosity of the total weld. The gravimetric measurements were made on three separate occasions to ensure accurate results. The calculated percent porosity was then averaged over the three measurements. The procedure used was as follows:

1) Prepared cross-section of the weld to determine the depth and width of the weld.
2) Machined off excess base metal.
3) Weighed weldment.
4) Weighed weldment suspended in water.
5) Calculated weldment density using Archimedes' principle.

$$\text{Weld Volume} = (WW\ (air) - WW\ (water))SVW$$

$$\text{Weld Density} = \frac{WW\ (air)}{\text{Weld Volume}}$$

where WW = Weld Weight
SVW = Specific Volume of Water (1 cc/gr)

6) Calculated weld porosity by:

$$\text{Percent Porosity} = 100\% \times \frac{P(base)-P(weld)}{P(base)}$$

where P(base) = Base Metal Density
P(weld) = Weld Density

D-7. Surface Absorption

The temperature difference of the sample prior to, and after irradiation was used to calculate the absorbed energy, q_a, with the following equation:

$$q_a = \text{mass} \times \text{specific heat} \times (T - T_i)$$

where T = final sample temperature after irradiation

T_i = initial sample temperature

Once the absorbed energy was found, the absorptivity, α, was calculated using:

$$\alpha = \frac{q_a}{q_i}$$

where q_i = incident energy

The above equations hold with the following assumptions:

1) Neglible conduction losses (sample insulated)
2) Neglible convection losses (no cover gas impingement)
3) Neglible radiation losses (low maximum sample temperature)

CHAPTER IV

RESULTS

A. Part A: Surface treatments and cover gas effects

A-1 Metallurgical

The depths, widths, and depth-to-width ratios from the four metallurgical cross sections of each weld were averaged and tabulated in Table IV-1. The averaged depth-to-width ratios were plotted and grouped by surface treatment and cover gas in Figures IV-1 and IV-2 respectively. Instrument air had the greatest depth-to-width ratios in all cases. The cover gases with hydrogen additions had no correlatable effect on the depth-to-width ratio. The weld pores were classified by type. Pore classification was determined by size and shape. Classifications are as follows:

Type 1 = Spherical 0.1 mm to 0.25 mm in diameter

Type 2 = Spherical 0.25 mm to 0.5 mm in diameter

Type 3 = Spherical > 0.5 mm in diameter

Type 4 = Non - spherical

Examples of each type are in Figures IV-3 and IV-4. The number of each type was averaged from the four metallurgical cross sections and plotted with respect to surface treatment and cover gas in Figures IV-5 and IV-6. When dry helium was used as the cover gas less pores were observed than for the other gases. The least pores were found when the

surface was sandblasted and dry helium was the cover gas. The blackened surfaces demonstrated less pores than the brushed surfaces in all cases.

A-2 Video

Representative photographs of the plasma images for each surface treatment and cover gas are in Figures IV-7 through IV-10. The shape of the laser induced plasma was similar for all gases and surface treatments, but those plasmas formed when an argon cover gas was employed were larger. The plasmas formed when argon was used were two times larger those with air and three to four times larger than those with helium based cover gases.

B. Part B: Plasma effects

B-1 OMA #1

The averaged spectrum of the plasma for each cover gas used is plotted versus wavelength in Figures IV-11 through IV-16. The averaged areas with thier respective standard deviations, in arbitary units, under the H_α peak from the 50 scans for each cover gas are listed in Table IV-2.

B-2 OMA #2

The plasma widths at the workpiece surface found from the averaged horizontal intensity data are listed in Table IV-2. The plasma widths, when argon-based cover gases are employed, are greater than those when a helium-based cover gas is used as indicated by the plasma video images.

B-3 Gravimetric

The averages of the percent porosity found from the three gravimetric measurements for each cover gas are listed in Table IV-2. The weld depth, width and depth-to-width ratio from the metallurgical cross section made in step one of the gravimetric measurement procedure are also listed in Table IV-2.

C. Surface Absorption

The thermal histories from the surface absorption runs for each of the surface treatments are plotted in Figures IV-17 through IV-20. The temperature rise for the repeated runs with polished, brushed, and sandblasted surfaces were almost identical. Also, the final sample temperature remained constant after irradiation; hence justifying the neglible conduction, convection and radiation losses assumptions. The detector was saturated during the first run with the blackened surface treatment, hence the gain was decreased for the second run. Upon completion of the second run on the blackened surface, the temperature did not remain constant as in the other runs, it declined. However, the temperature losses were less than two degrees per second after irradiation; thus justifying the assumptions stated above. The absorptance, at room temperature, for the polished, brushed, blackened, and sandblasted surface treatments were 0.029, 0.060, 0.734, and 0.217 respectively.

CHAPTER V

DISCUSSION

A. Depth to Width Ratio vs. Surface Treatment

The depth to width (D/W) ratio is a measure of deep penetration welding, with values greater than one being desirable. Depth to width ratios of the polished surface treated specimens were the least affected by changes in the cover gas. The brushed, and blackened surfaces demonstrated similar patterns of response to the different cover gases with the blackened having the greatest D/W ratios of the two. The blackened surfaces showed the greatest D/W ratio for air, dry argon, and wet argon; surprisingly, this did not occur with the helium based cover gases. In the latter case, the sandblasted surfaces produced the greater penetration.

B. Depth to Width Ratio vs. Cover Gas

Cover gases with increased amounts of hydrogen (Wet Argon & He 5% H_2) had no correlatable effect on the D/W ratios. For every surface finish, the greatest D/W ratio was obtained using air as the cover gas. This can be attributed to the fact that air is a reactive gas (e.g. non-inert) containing nitrogen and oxygen. The welding process is enhanced by an exothermic chemical reaction between aluminum and nitrogen.[21] The chemical reaction forms an Al-N-O ternary compound layer at the surface. The

absorption of the system Al and Al-N-O is higher than the absorption of an oxidized aluminum surface.[21]

C. Porosity vs. Surface Treatment

The surface treatment had an effect on the type of pore formed. This stands to reason since the surface finish influences the amount of energy absorbed, and thus effects the solidification morphology and the bubble growth. The blackened surfaces demonstrated less type 1 porosity than did either the brushed or sandblasted surfaces for the same cover gas. This trend is reasonable in that the blackened surfaces absorbed more of the incident energy than the roughened surfaces thereby increasing the convection in the weld pool. The increased convection would facilitate the escape of the hydrogen bubbles from the molten metal, hence reducing porosity. The polished surface welds all demonstrated type 4 porosity irrespective of the cover gas used, indicating a possible porosity formation mechanism other than hydrogen gas entrapment.

D. Porosity vs. Cover Gas

The cover gas influenced the quantity of pores formed, since the cover gas is the most abundant source of hydrogen to the weld pool. The amount of hydrogen in the weld pool, along with the nuceation sites, will dictate the nucleation rate of hydrogen bubbles and hence the quantity of pores.

The porosity levels in the welds performed under wet argon were higher than those where He 5% H_2 was used, even

though He 5% H_2 contains more hydrogen. At first glance, this appears to be in conflict with theory. However, when the weld pool widths and plasma sizes are considered this phenomena is explainable. Weld porosity was found to be a function of weld pool surface area (in conventional welding) by R. A. Woods[13]. Woods also found that the weld porosity was a function of arc length, which dictates the arc volume, and arc volume is analogous to the plasma volume. The volume of the plasma is a function of plasma width at the workpiece. Larger weld pool widths where produced when wet argon was used, compared to He 5% H_2, as the cover gas in all cases except the blackened surface treatment. In all cases, the plasma generated with wet argon was larger than the plasma generated with He 5% H_2 (See Figures IV-7 through IV-10). The transfer of atomic hydrogen would then be greater in the weld pools under a wet argon weld plasma than those under He 5% H_2.

E. Video vs. Surface Treatment & Cover Gas

The plasma images indicate that the surface treatment had little effect on the plasma size. The plasma size did appear to be dependent on the cover gas used. For example, as mentioned above, the plasma generated was larger with wet argon as the cover gas than He 5% H_2. Hence the plasma size is more dependent on the base cover gas used (Ar or He), rather than the form of hydrogen contamination (moisture or H_2).

F. OMA vs. Porosity

When the averaged areas under the H_α peak from the 50 spectra are normalized and plotted versus the average percent porosity from the gravimetric measurements for each cover gas, linear relationships are seen for the argon and helium based cover gases (Figures V-1 and V-2). The error bars in the direction of the area under the H_α peak are the standard deviations of the normalized areas. The error bars in the percent porosity direction is the error associated with the gravimetric technique, which is approximately $\pm$5%. The argon and helium based cover gases were plotted separately due to the disparity between the sizes of the plasma generated with these cover gases.

G. Comparison to previous work

Both Woods[13] and Martukanitz[9] found that in Al 5083 additions as small as 0.12% H_2 to the cover gas produced welds with four to six percent porosity. Also, as concentrations of hydrogen increased to 0.3% the amount of porosity increased to 16%[9,13]. In the laser welding study presented herein the addition of 5% H_2 to the cover gas produced welds with about five percent porosity after laser processing. As evidenced by Figure V-1, increasing amounts of hydrogen lead to higher levels of porosity in a linear fashion when a helium based cover gas is used. This is in agreement with the previosly mentioned studies.

H. Thermal Absorption - Surface Reflectivity

The absorptivity is defined as the fraction of the energy incident on the sample that is absorbed by the sample.[28] Assuming that all of the incident energy is either absorbed or reflected, the temperature rise of the sample can be used to find the reflectivity from the absorptivity. The percent reflectivity for polished, brushed, blackened, and sandblasted surfaces of Al 5083, at room temperature, are therefore 97.1%, 94.0%, 26.6%, and 78.3%, respectively. The theoretical reflectivity of an ideally polished aluminum surface is 99%; however, with the experimentally polished surface one would expect a lower reflectivity due to imperfections on the surface. Thus a reasonable estimate of the error associated with these experimental measuremants is 5%.

The advantage of the experimental method used in this project as compared to that used by Arata is the direct measurement of the sample temperature rise during irradiation. However, this technique also includes a disadvantage, namely, the sample temperature will cause the absorption coefficient of the sample to change. The error introduced by this mechanism can be neglected if the sample temperature does not approach its melting point.

CHAPTER VI

CONCLUSIONS

The following conclusions can be made as a result of the laser beam welds performed on Al 5083 with different surface treatments and various cover gases:

1. The laser weld porosity in Al 5083 was affected by the same influences as conventional weld porosity; plasma hydrogen content (arc hydrogen content), plasma volume (arc volume), and weld pool surface area.
2. The cover (or shield) gases used were a major influence in the formation of laser weld porosity due to their influence on the size of the plasma.
3. The pore size was influenced by both the cover gas and surface treatment, in that both affected the solidification morphology through the weld thermal cycle. The cover gases containing hydrogen produced the largest pores (type 4). The polished surface treatment produced type 4 porosity irrespective of cover gas used.
4. The spectrally monitored weld plasma could detect the presence of hydrogen. The area under the H_α peak was an indicator of the amount of weld porosity formed for a given cover gas, in that a greater area under the peak resulted in greater porosity.

5. The amount of porosity formed for a given amount of added hydrogen in the cover gas was less during laser welding than for conventional welding.
6. The room temperature reflectivity of Al 5083 to 10.6 μm radiation was a function of the surface treatment and the lowest reflectivity resulted from brushing and blackening the surface with carbon soot.
7. The reflectivity of the surface was proportional to its degree of smoothness when a coating was not used, thus the polished (smoothest) was the most reflective and the sandblasted (roughest) was the least reflective.
8. The size of the laser induced plasma during laser welding was dependent primarily on the cover gas species rather than the surface treatment and was largest for argon and smallest for helium.
9. The weld with the least pores was obtained using helium as the cover gas and sandblasting as the surface treatment.

Since porosity formed for a given amount of hydrogen appears to be different for conventional and laser welding, the investigation of this phenomena would be possible with a series of laser welds with either custom pre-mixed cover gases (cheapest) or by making hydrogen additions to the cover gas using a manifold (most dangerous and accurate).

LIST OF REFERENCES

[1] E.F.Nippes,Metals Handbook, 9th Edition, Vol. 6 (Welding,Brazing, and Soldering), p.826, 1986.

[2] A. Blake, J. Mazumder, "Control of Magnesium Loss During Laser Welding of Al-5083 Using a Plasma Suppression Technique", Journal of Engineering for Industry, Vol. 107, p. 275, August 1985.

[3] J.Mazumder, Laser Welding: State of the Art Review", Journal of Metals, p.18, July 1982.

[4] M. H. McCay et al, "Correlation of Plasma Characteristics with Weldment Properties for Laser Welded Aluminum Alloys", Internal Report, Center for Laser Applications, University of Tennessee Space Institute, Tullahoma, Tennesse.

[5] Ref. [1] p.26

[6] Ref. [1] p.153

[7] Ref. [1] p.182

[8] Ref. [1] p.842

[9] R. P. Martukanitz, R. Michnuk, "Sources of Porosity in Gas Metal Arc Welding of Aluminum," Alcoa Report No. 53-81-4,Alcoa Laboratories, Alcoa Center, PA, 15069, May 21, 1981.

[10] Ref. [9] p.278

[11] J.H.Devletian,W.E.Wood,"Factors Affecting Porosity in Aluminum Welds-A Review", Welding Research Council Bullitin No. 260, p.1, December 1983.

[12] Ref. [11] p.3

[13] R.A.Woods, "Porosity and Hydrogen Absorption in Aluminum Welds", Welding Research Supplement, March 1974.

[14] Z.P.Saperstien et al, "Porosity in Aluminum Welds", Welding Research Supplement, October 1962.

[15] Ref. [3] p.16

[16] Arata, Plasma, Electron, & Laser Beam Technology, p.351, ASM Metals Park OH, 1986.

[17] M.B.C.Quigley, "High Power Density Welding", The Physics of Welding, Chp.8, Pergamon Press, 1984.

[18] G.K.Lewis, R.D.Dixon, "Plasma Monitoring of Laser Beam Welds", Welding Research Supplement, p.49-s, February 1985.

[19] I. Miyamoto, "Beam Absorption Mechanism in Laser Welding", p.11, SPIE Vol. 668, Laser Processing: Fundamentals, Applications, and Systems Engineering, 1986.

[20] Ref. [14] p.263

[21] K.Behler, et al, "Laser Welding of Aluminum", Proceedings of the 7th International Congress on Applicatios of Lasers and Eletrooptics ICALEO '88 Gerald Bruck (editor), Santa Clara, CA, USA.

[22] Ref. [16] p.408

[23] Ref. [16] p.498

[24] Ref. [16] p.405

[25] Conversations with Dr.T.D.McCay on July 20, 1990.

[26] Ref. [16] p.237

[27] Ref. [16] p.234

[28] R.Siegel and J.R.Howell, Thermal Radiation Heat Transfer, p.55, Hemispherical Publishing Corporation, N.Y. N.Y., 1981.

APPENDIXES

APPENDIX A

LIST OF SYMBOLS AND

ABBREVIATIONS

CID.....Charge Injected Device

CW.....Continuous Wave

D/W.....Depth to Width Ratio

eV.....Electron Volt

GMA.....Gas Metal Arc (Welding)

GTA.....Gas Tungsten Arc (Welding)

K.....Partition

LBW.....Laser Beam Welding

LOF.....Lack of Fusion

LOP.....Lack of Penetration

mm.....millimeter (10^{-3} meters)

ND.....Neutral Density

OMA.....Optical Multichannel Analyzer

P.....Density

PC.....Personal Computer

ppm.....parts per million

q_a.....Absorbed Energy

q_i.....Incident Energy

RF.....Radio Frequency

SVW.....Specific Volume of Water

T.....Final Sample Temperature

T_i.....Initial Sample Temperature

fm.....micrometer (10^{-6})

APPENDIX B

TABLES AND FIGURES

Table II-1. **Composition Al 5083**

Element	Weight %
Mg	4.45
Mn	0.70
Cr	0.15
Al	remainder

Table II-2. **Properties Al 5083**

Density.....2.66 g/cc
Specific Heat.....900 J/kg K
Thermal Conductivity.....120 W/m K
Liquidus.....638 C
Solidus.....574 C
Vaporization Temperature.2476 C (Al)
Vaporization Temperature.1107 C (Mg)
Vapor Pressure @ 1000 C..2.8 x 10^{-7} (Al)
Vapor Pressure @ 1000 C..7 x 10^{-1} (Mg)
Ionization potential.....5.986 eV (Al)
Ionization potential.....7.646 eV (Mg)

Table III-1. **Study Matrix** (Part A)

Instrument Air	Polish A1	Brushed A10	Blackened A11	Sandblasted A20
Argon	A2	A9	A12	A19
Wet Ar	A3	A8	A13	A18
Helium	A4	A7	A14	A17
He-5%H_2	A5	A6	A15	A16

Table III-2. **Study Matrix** (Part B)

Surface Finish = Brushed	
He-5%H_2	B1
Argon	B2
Helium	B3
Wet He	B4
Wet Ar	B5
Wet He-5%H_2	B6

Table III-3. **Weld Parameters** (Parts A & B)

Power = 2300 Watts

Mode = 'Quasi' - CW

Speed = 25 mm/sec

Focus = 2.5 mm below surface

Standoff = 7 mm

Gas Flow = 4.1 lt/min (air)
3.4 lt/min (argon)
11.0 lt/min (helium)
11.9 lt/min (He-5%H_2)

Table III-4. **Gas Properties**

	Air	Water Vapor	Argon	Helium	Hydrogen
Ionization Potential (eV)	N_2 14.534 O_2 13.618		15.76	24.587	13.598
Thermal Conductivity (cal/cm sec K)	$.622 \times 10^{-4}$	$.53 \times 10^{-4}$	$.43 \times 10^{-4}$	3.6×10^{-4}	4.46×10^{-4}
Density (relative to air)	1.0	1.02	1.38	0.137	0.070

Table IV-1. **Averaged weld depths, widths, and areas**(Part A)

Run	Depth(mm)	Width(mm)	D/W ratio	Area(mm sq.)
A1	3.24	3.38	0.96	5.46
A2	2.50	3.10	0.81	3.88
A3	2.35	3.06	0.77	3.60
A4	2.49	2.84	0.88	3.53
A5	2.23	2.58	0.86	2.86
A6	2.58	3.11	0.83	4.01
A7	2.08	3.03	0.69	3.14
A8	2.43	3.14	0.77	3.80
A9	2.56	2.86	0.90	3.67
A10	2.88	3.03	0.95	4.35
A11	3.41	2.88	1.19	4.91
A12	2.79	2.81	0.99	3.92
A13	2.58	3.00	0.86	3.86
A14	2.10	2.98	0.71	3.12
A15	2.83	3.40	0.83	4.80
A16	2.59	2.88	0.90	3.72
A17	2.41	2.60	0.93	3.14
A18	2.73	3.19	0.85	4.34
A19	1.95	2.96	0.66	2.88
A20	3.64	3.25	1.12	5.91

Table IV-2. **Results** (Part B)

Area under Hα Peak (pixel sq.) (from OMA 1)

Run	Mean	Standard Deviation	
B1	11,922	3,745	(He-5%H_2)
B2	106,281	31,282	(Ar)
B3	4,121	1,727	(He)
B4	9,894	2,747	(Wet He)
B5	205,635	127,189	(Wet Ar)
B6	17,886	6,871	(Wet He-5%H_2)

Plasma Widths (mm) (from OMA 2)

Run	Mean	Standard Deviation	
B1	2.211	0.1255	(He-5%H_2)
B2	3.155	0.2656	(Ar)
B3	2.079	0.0838	(He)
B4	2.174	0.0833	(Wet He)
B5	2.591	0.1656	(Wet Ar)
B6	2.070	0.0492	(Wet He-5%H_2)

Percent Porosity (Gravimetric)

Run	Mean	Standard Deviation	
B1	5.403	0.0789	(He-5%H_2)
B2	3.255	1.298	(Ar)
B3	1.250	0.261	(He)
B4	3.880	1.094	(Wet He)
B5	6.735	1.539	(Wet Ar)
B6	8.946	2.789	(Wet He-5%H_2)

Weld Depths and Widths (mm)

Run	Depth	Width	D/W ratio	
B1	2.50	2.60	0.96	(He-5%H_2)
B2	2.20	3.00	0.73	(Ar)
B3	2.20	2.50	0.83	(He)
B4	2.50	2.50	1.00	(Wet He)
B5	2.00	3.00	0.67	(Wet Ar)
B6	2.50	2.75	0.91	(Wet He-5%H_2)

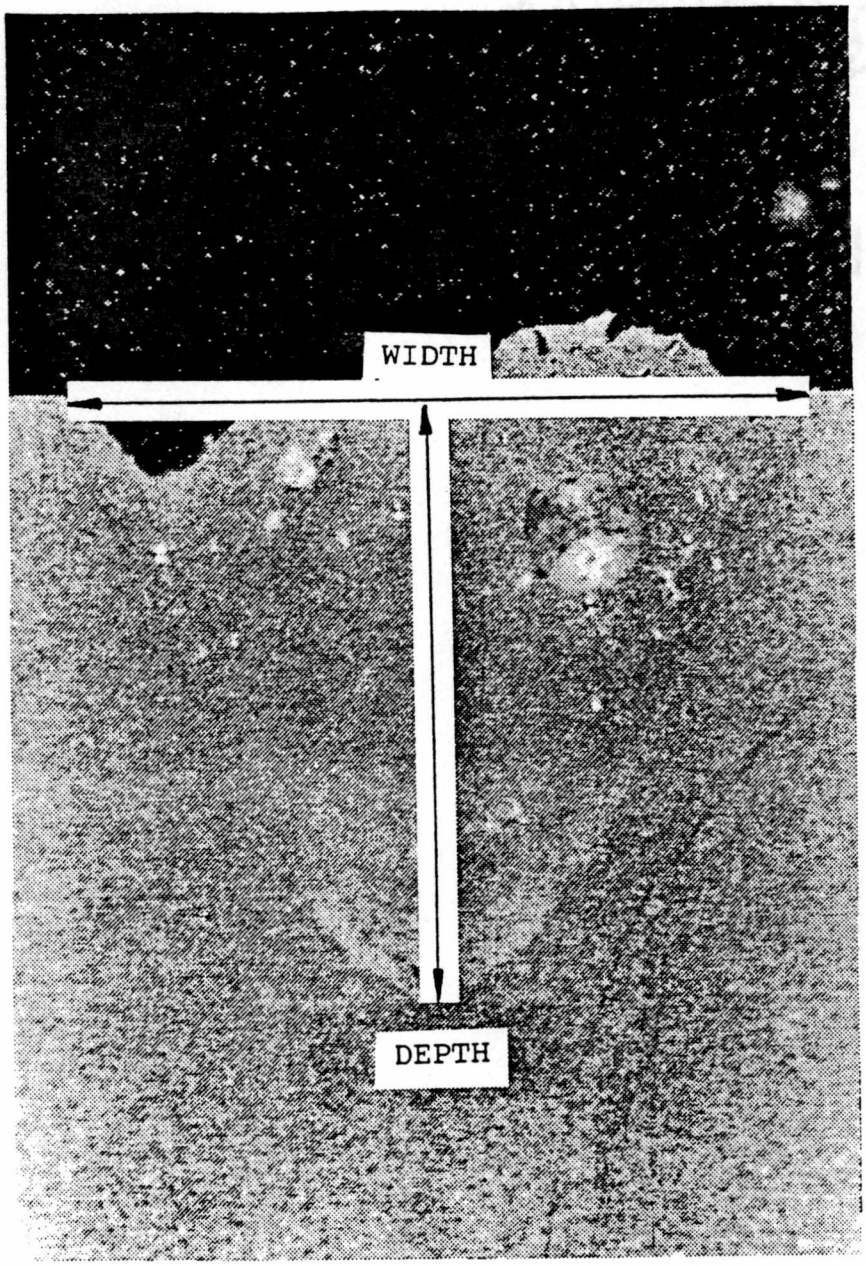


Figure II-1. Depth to Width Ratio.

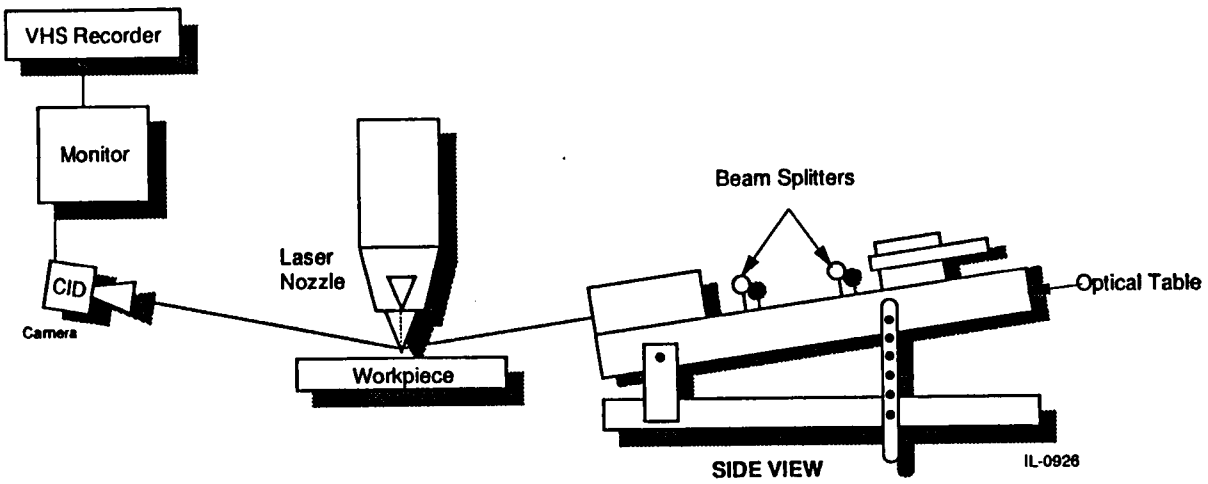


Figure III-1. Schematic drawing of instrument set-up.

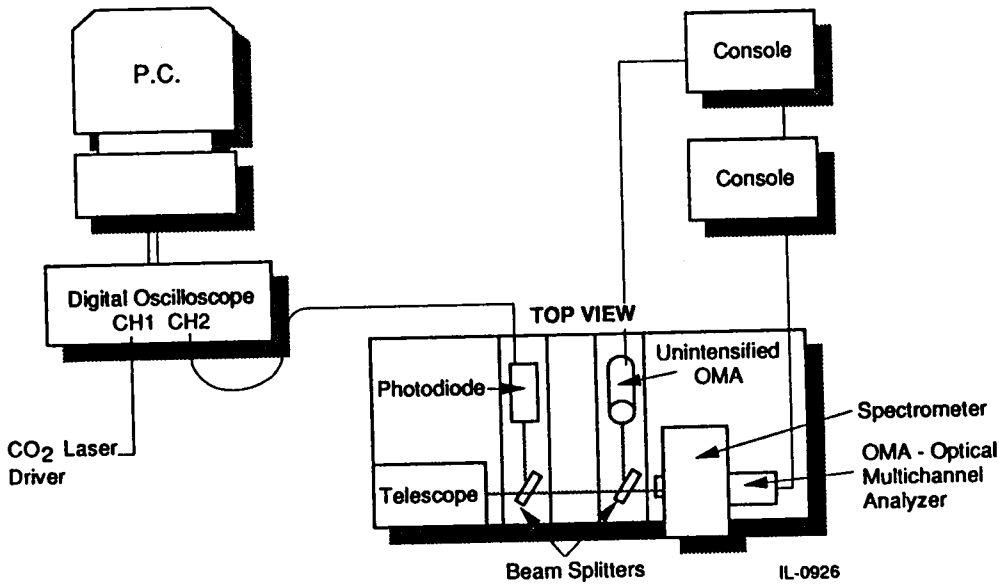


Figure III-2. Schematic drawing of optical table.

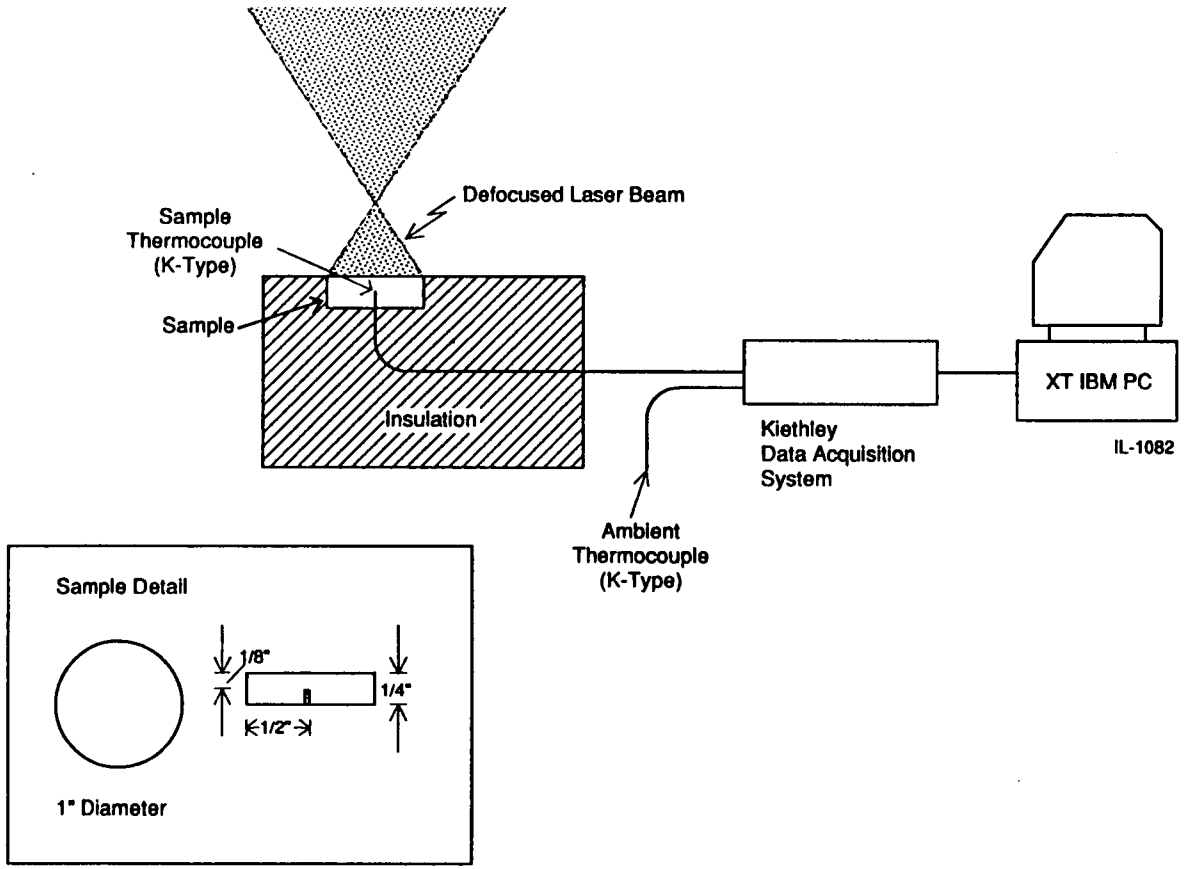
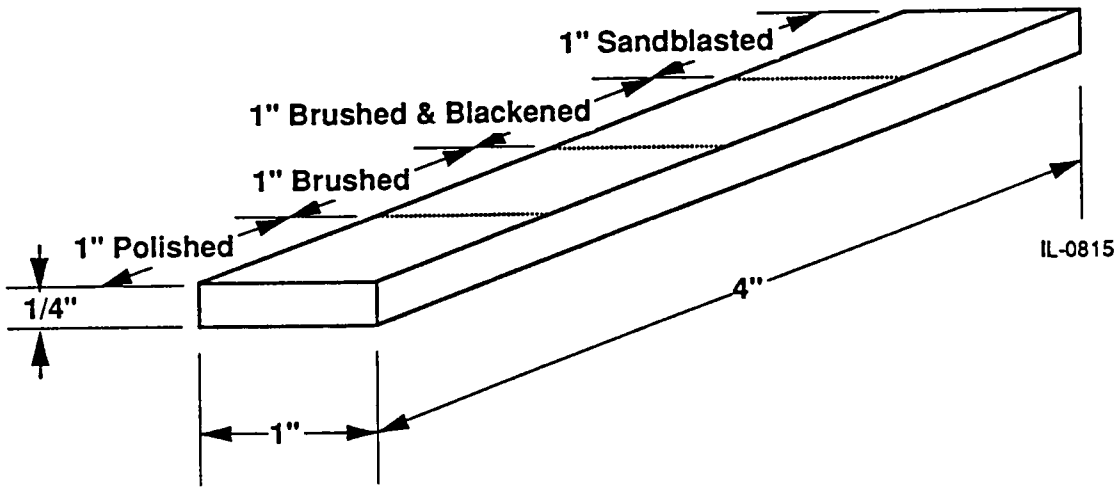


Figure III-3. Schematic drawing of experimental arrangement for the thermal absorption runs with a detail of the sample.



Schematic of Typical Al 5083 Sample with Surface Finish Treatments

Figure III-4. Schematic drawing of Al 5083 sample with surface finish treatments.

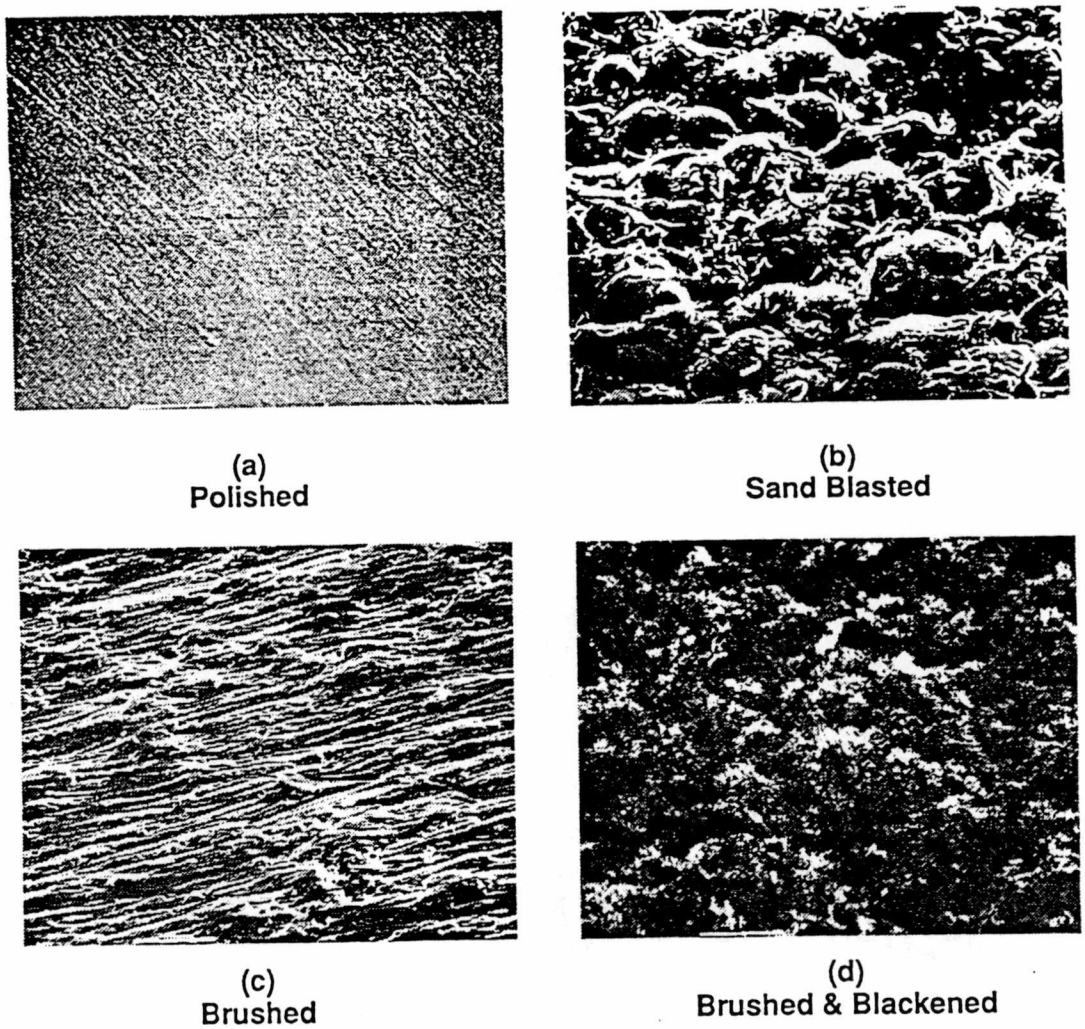


Figure III-5. Scanning electron micrographs of Al 5083 surface finishes (300X).

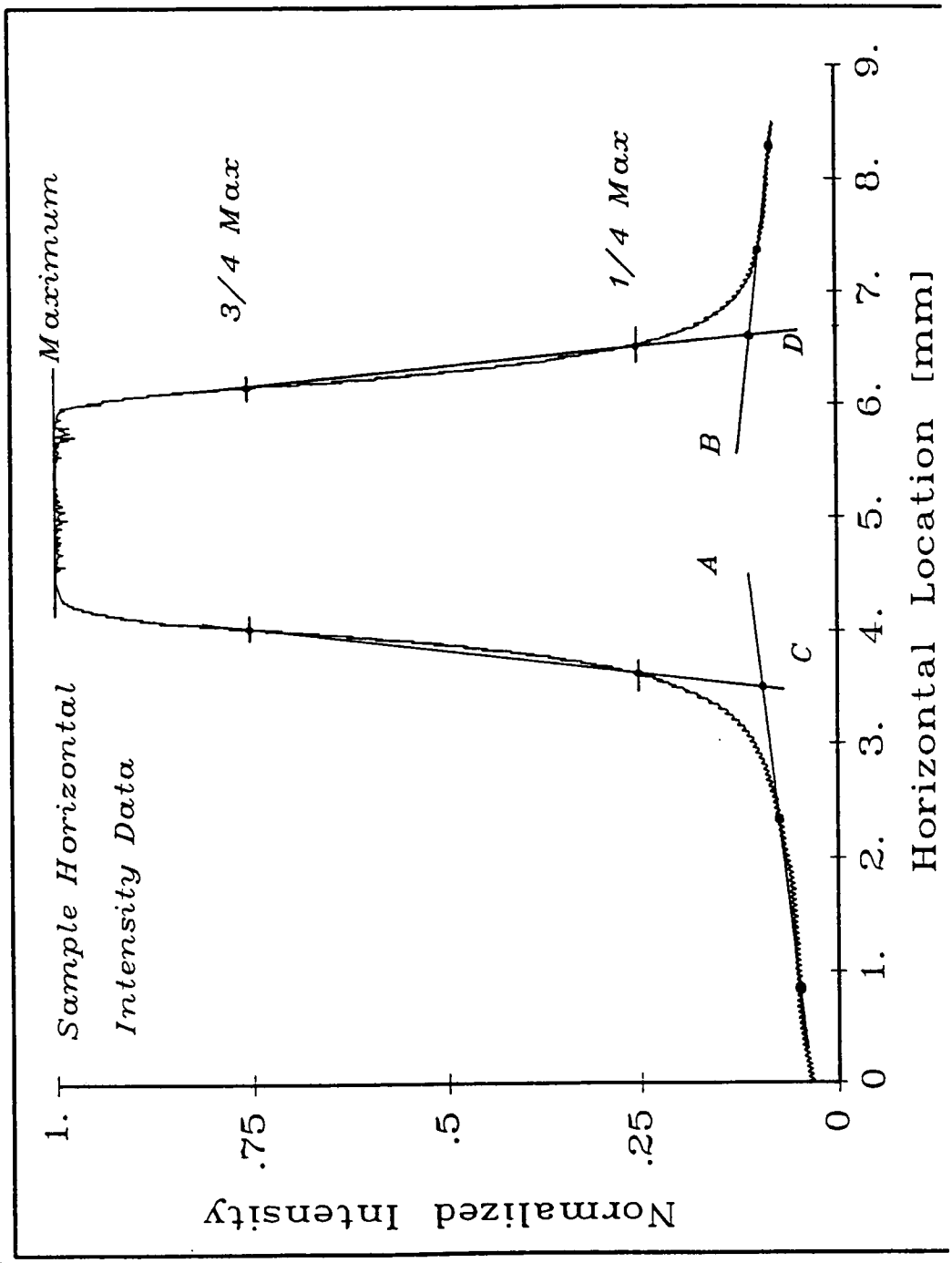


Figure III-6. Sample horizontal intensity data illustrating plasma width determination.

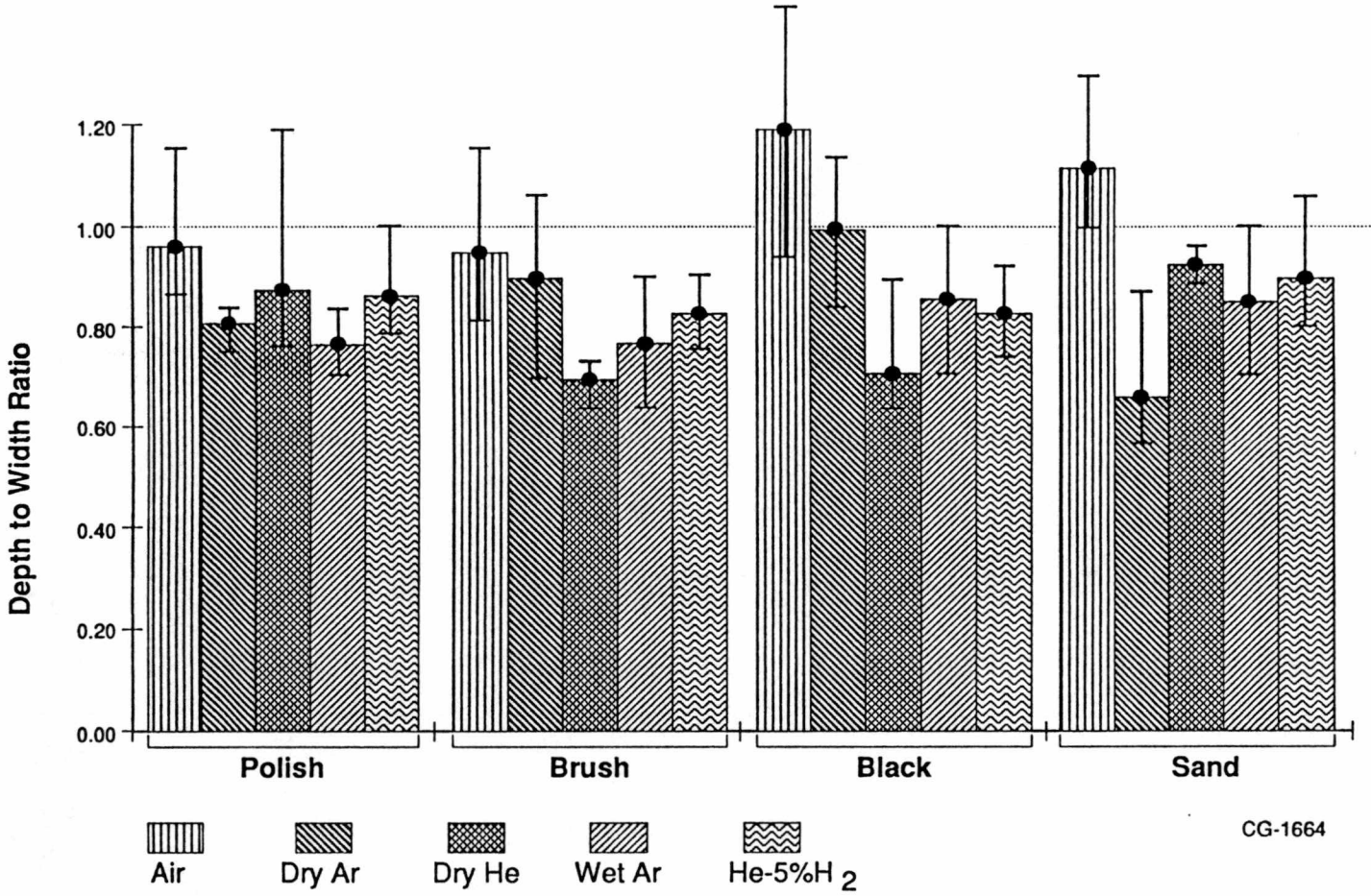


Figure IV-1. Averaged depth to width ratios from 'A' runs grouped by surface treatment. (Bars indicate maximum and minimum values).

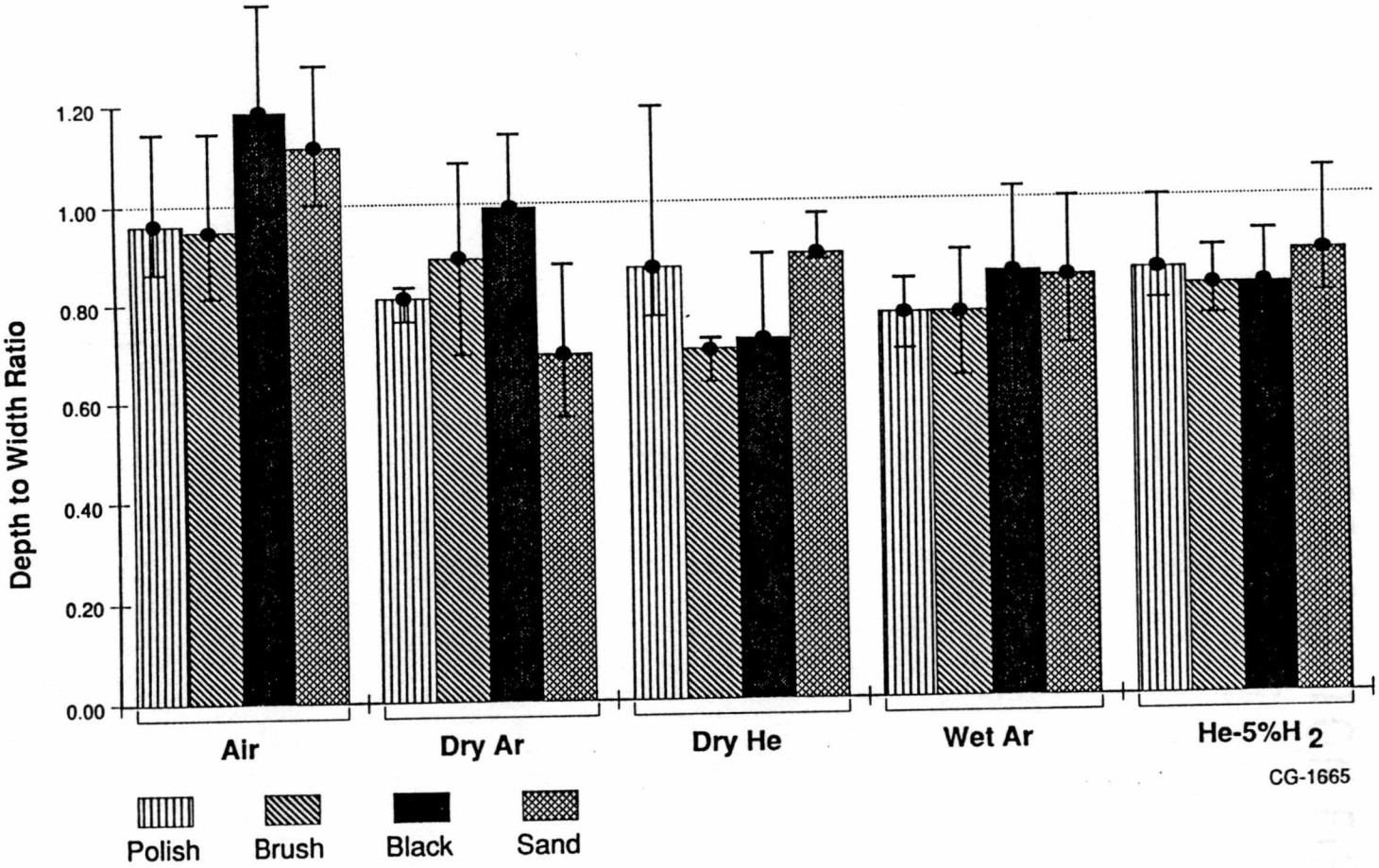


Figure IV-2. Averaged depth to width ratios from 'A' runs grouped by cover gas. (Bars indicate maximum and minimum values).

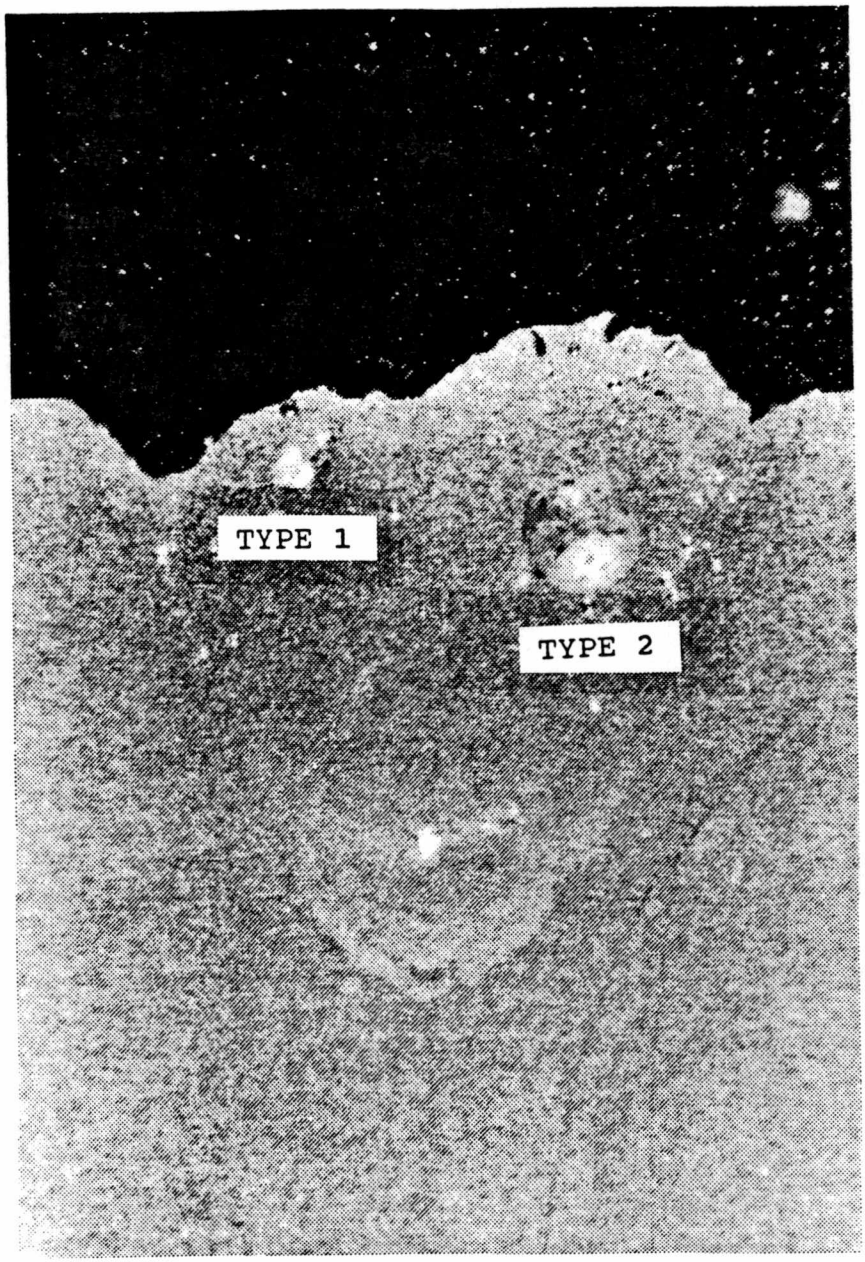


Figure IV-3. Example of type 1 and type 2 porosity.

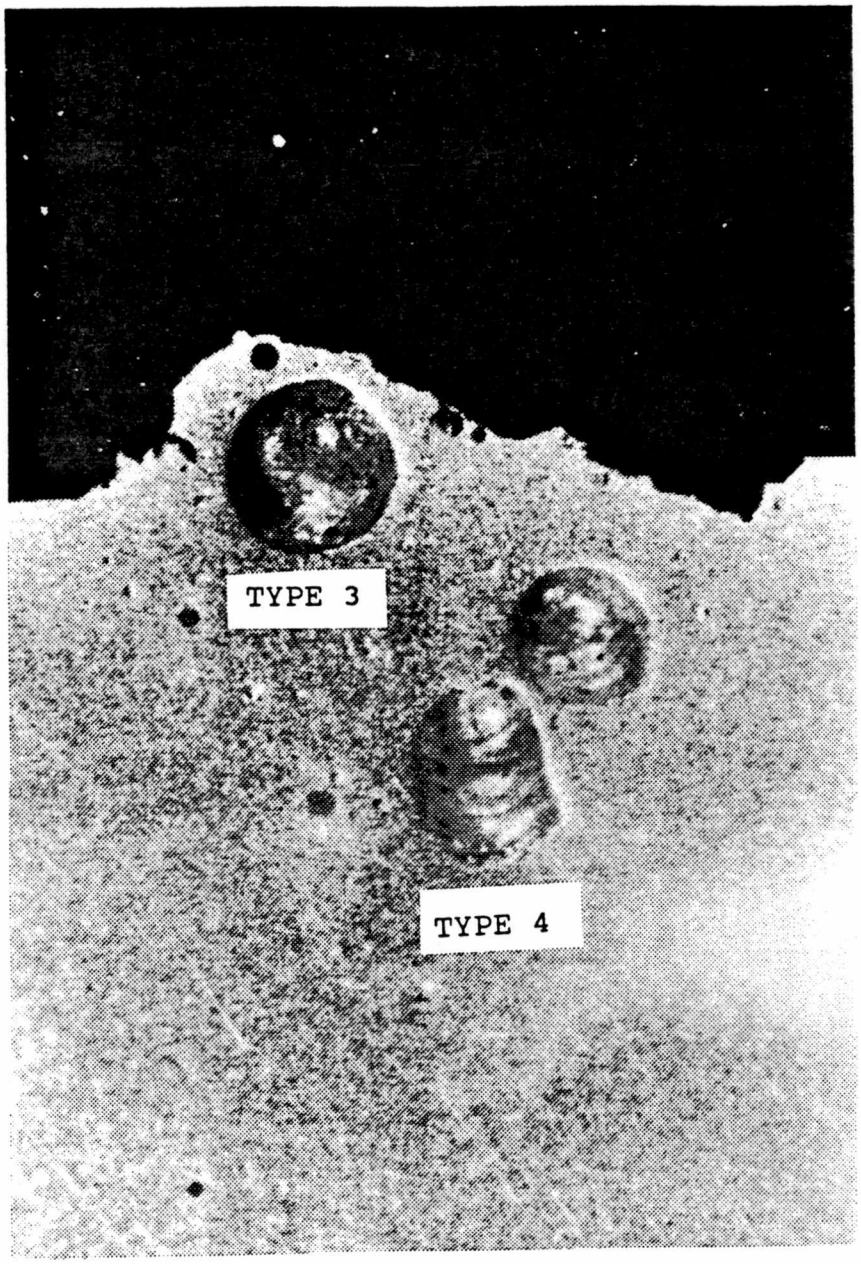


Figure IV-4. Example of type 3 and type 4 porosity.

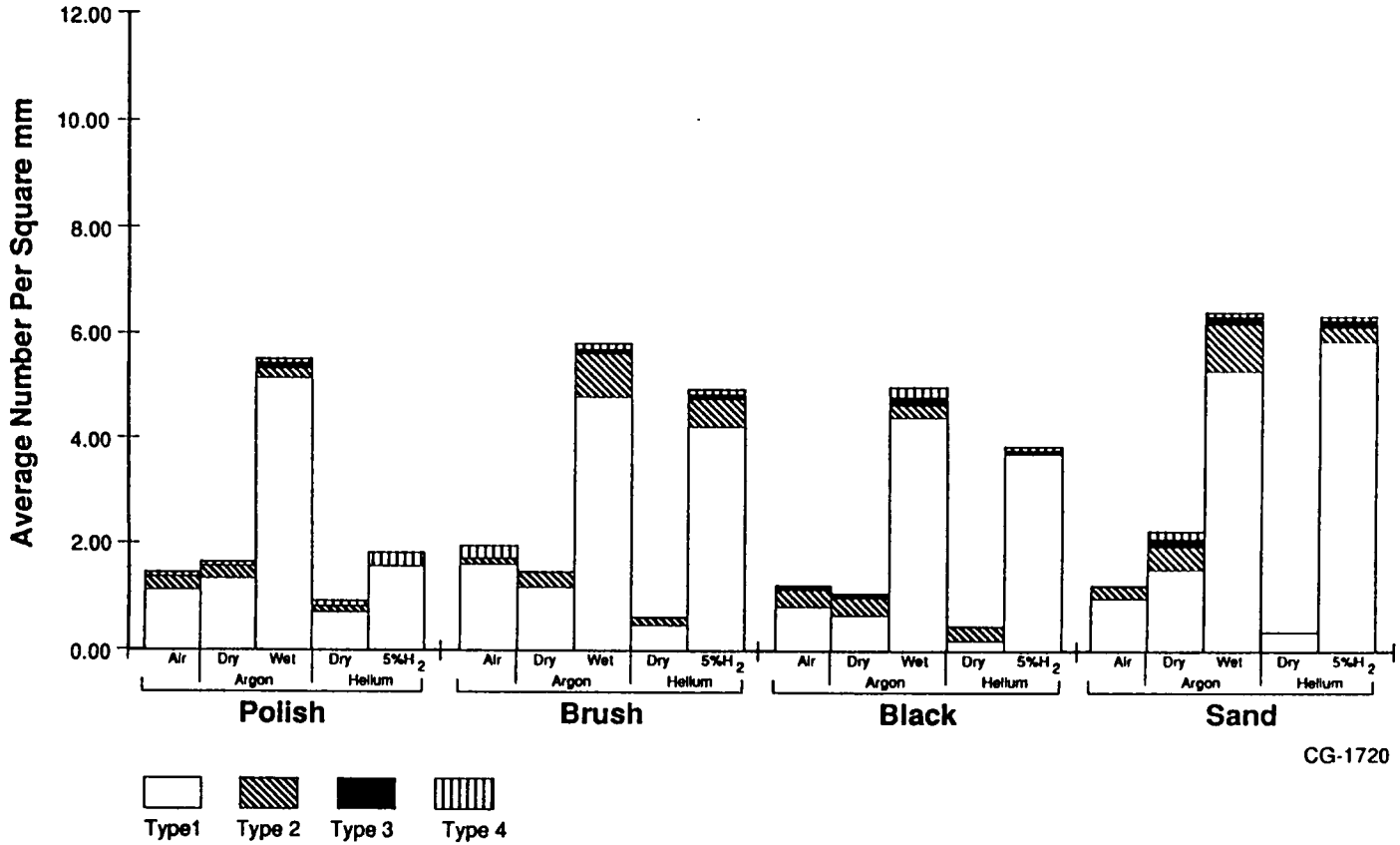


Figure IV-5. Average pores per square mm from 'A' runs grouped by surface finish.

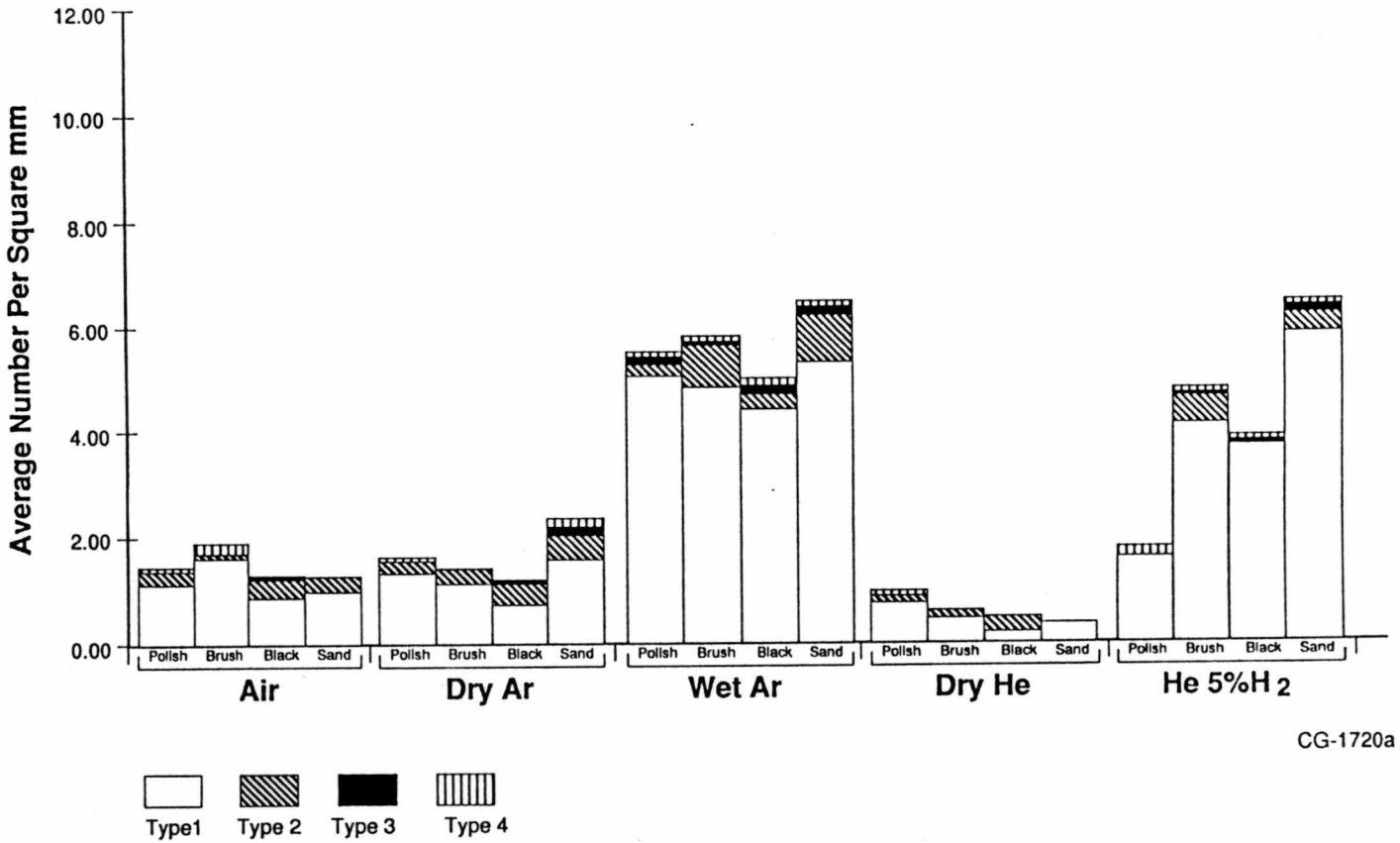
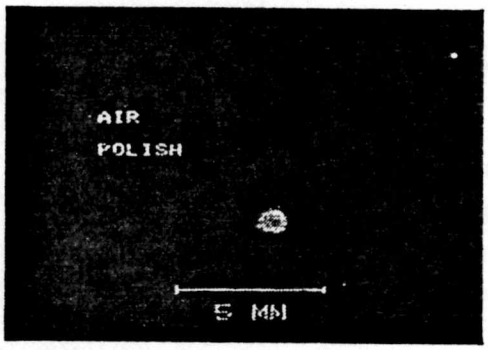
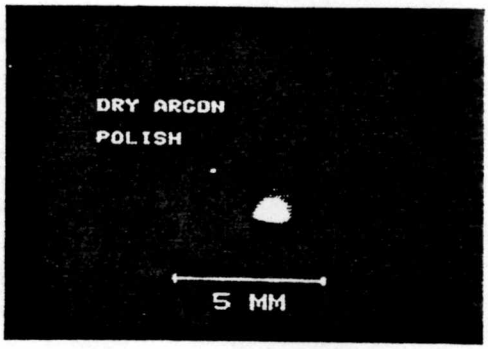


Figure IV-6. Average pores per square mm from 'A' runs grouped by cover gas.



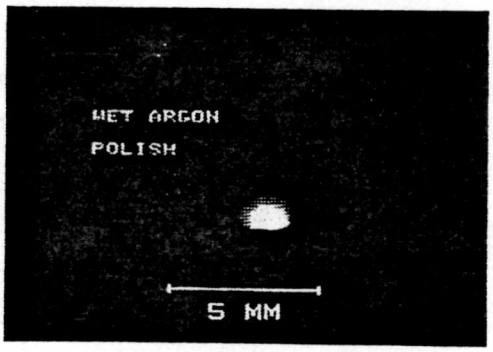
a. Air



b. Dry Argon



c. Dry He



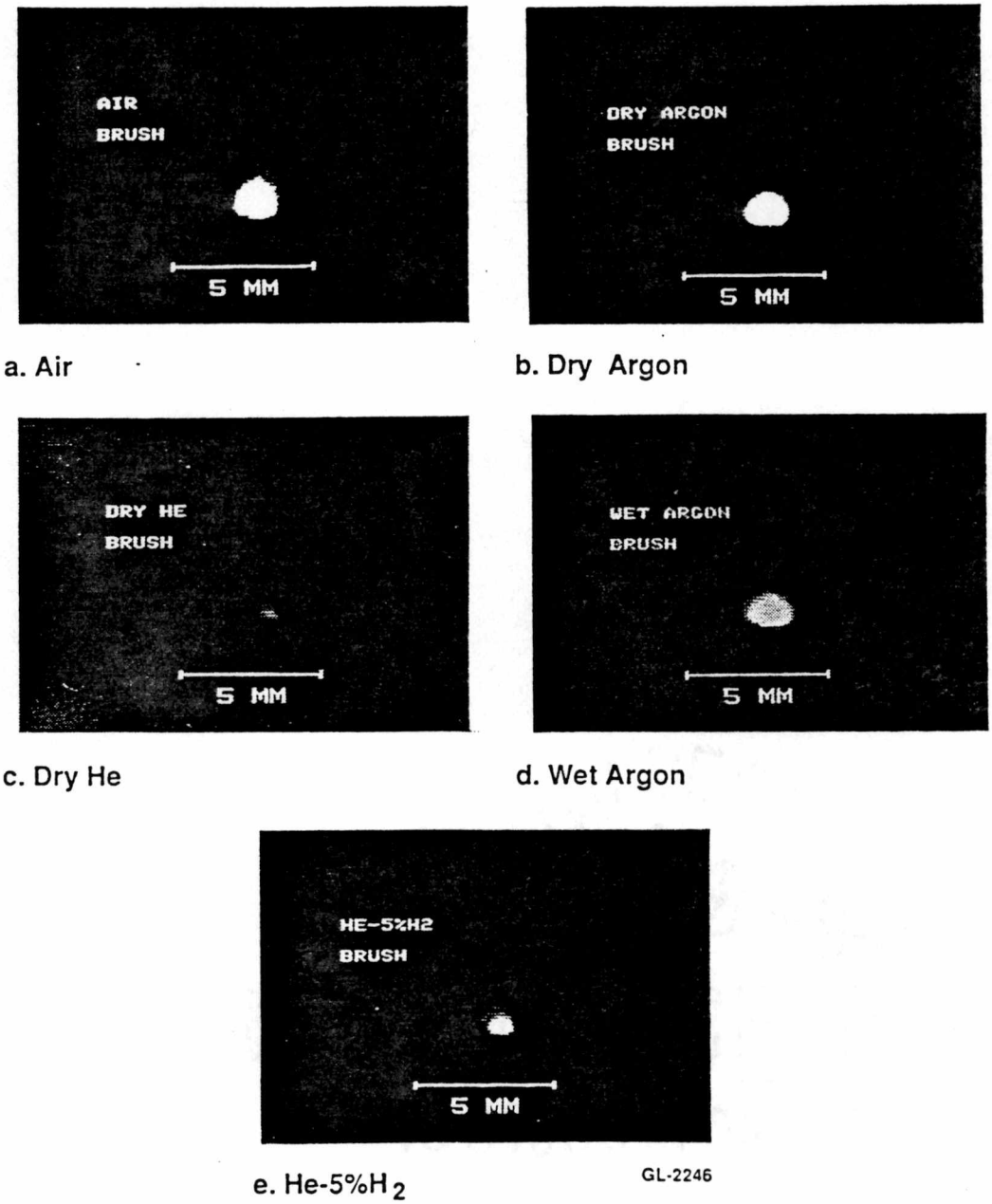
d. Wet Argon



e. He-5%H_2

GL-2243

Figure IV-7. Laser induced plasma over polished Al 5083 for various gases.



a. Air

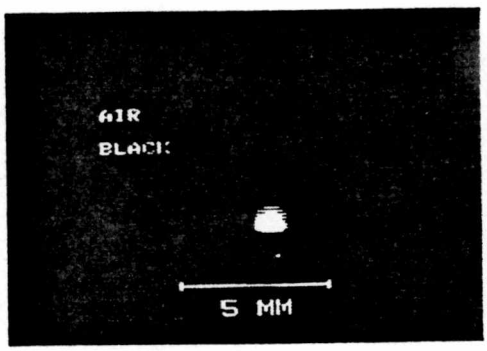
b. Dry Argon

c. Dry He

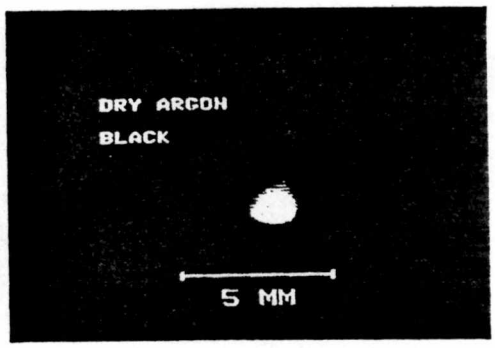
d. Wet Argon

e. He-5%H_2

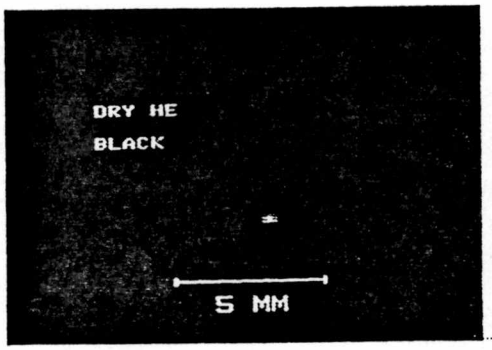
Figure IV-8. Laser induced plasma over brushed Al 5083 for various gases.



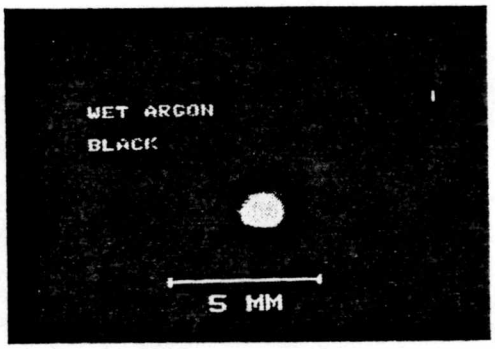
a. Air



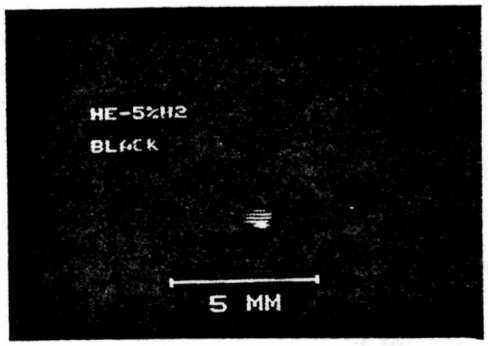
b. Dry Argon



c. Dry He



d. Wet Argon



e. He-5%H_2

GL-2244

Figure IV-9. Laser induced plasma over blackened Al 5083 for various gases.

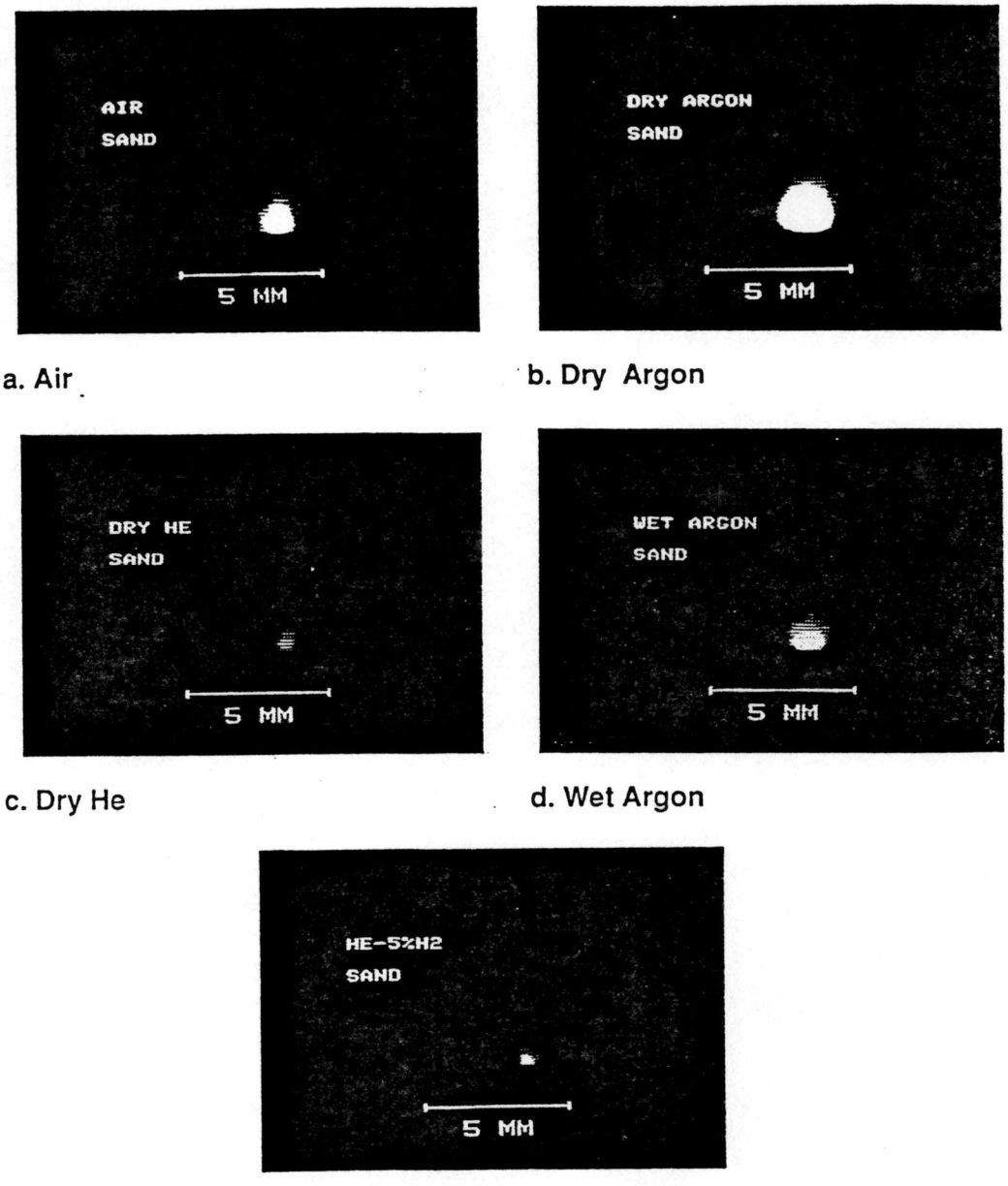


Figure IV-10. Laser induced plasma over sandblasted Al 5083 for various gases.

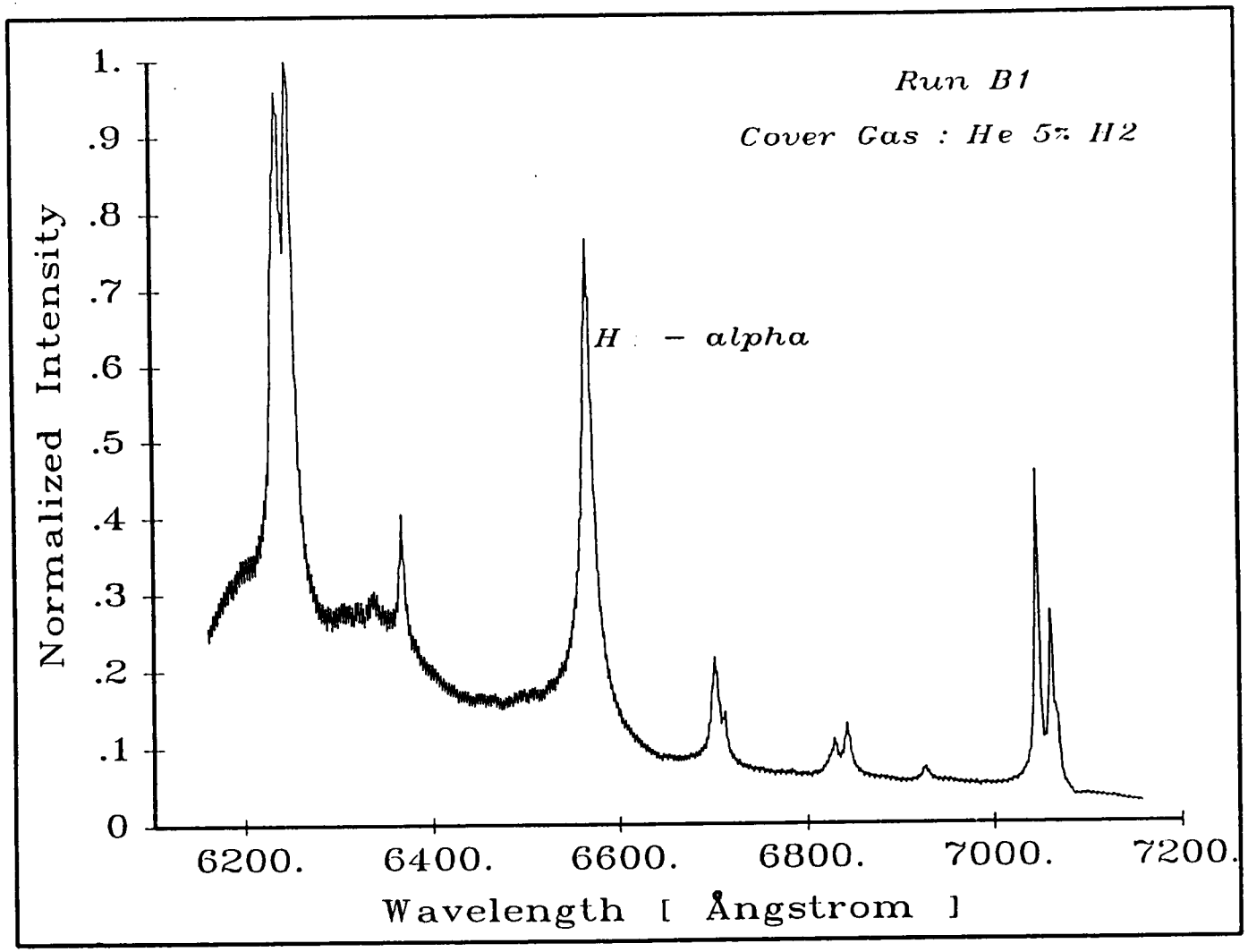


Figure IV-11. Averaged spectrum of plasma with He 5% H_2.

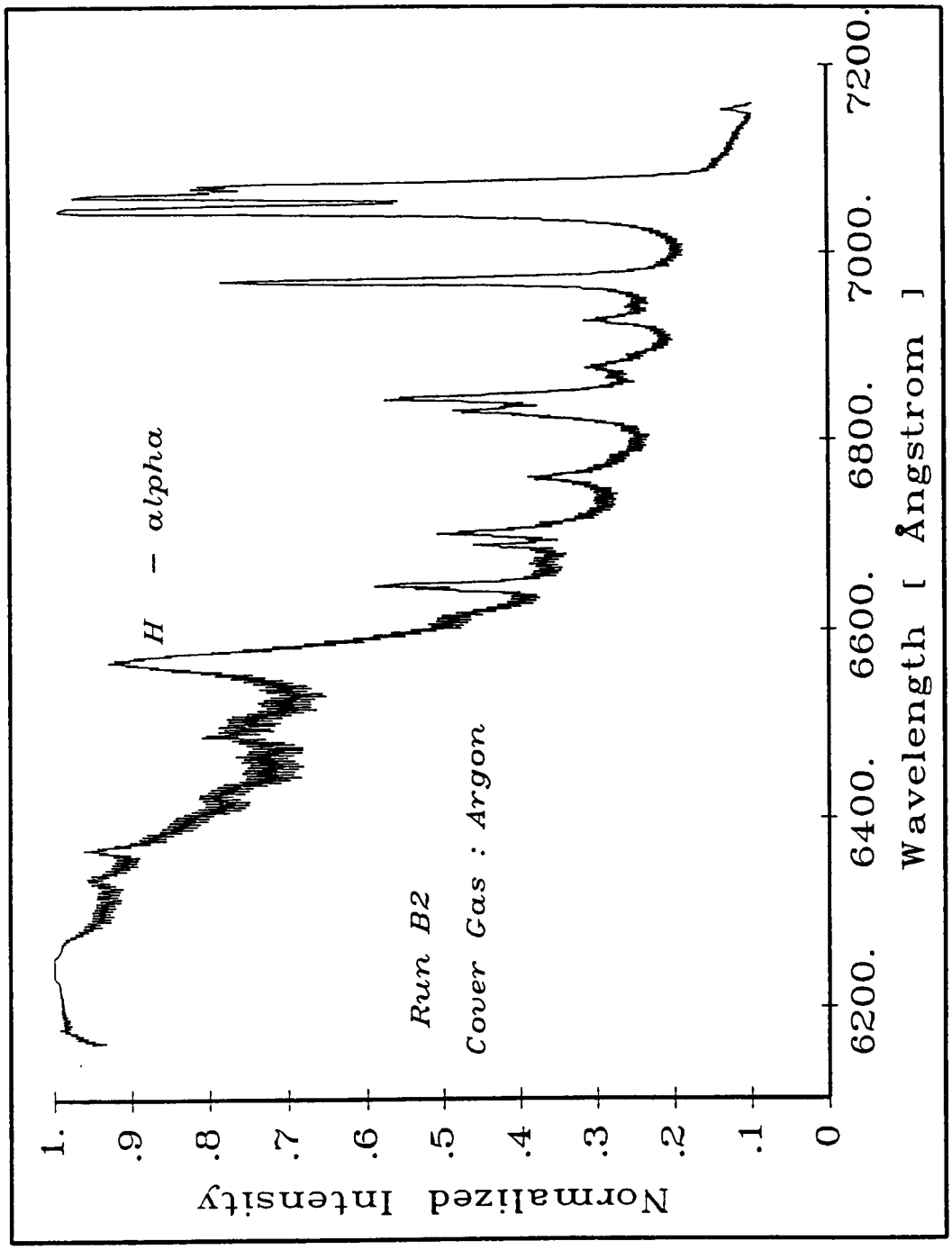


Figure IV-12. Averaged spectrum of plasma with argon.

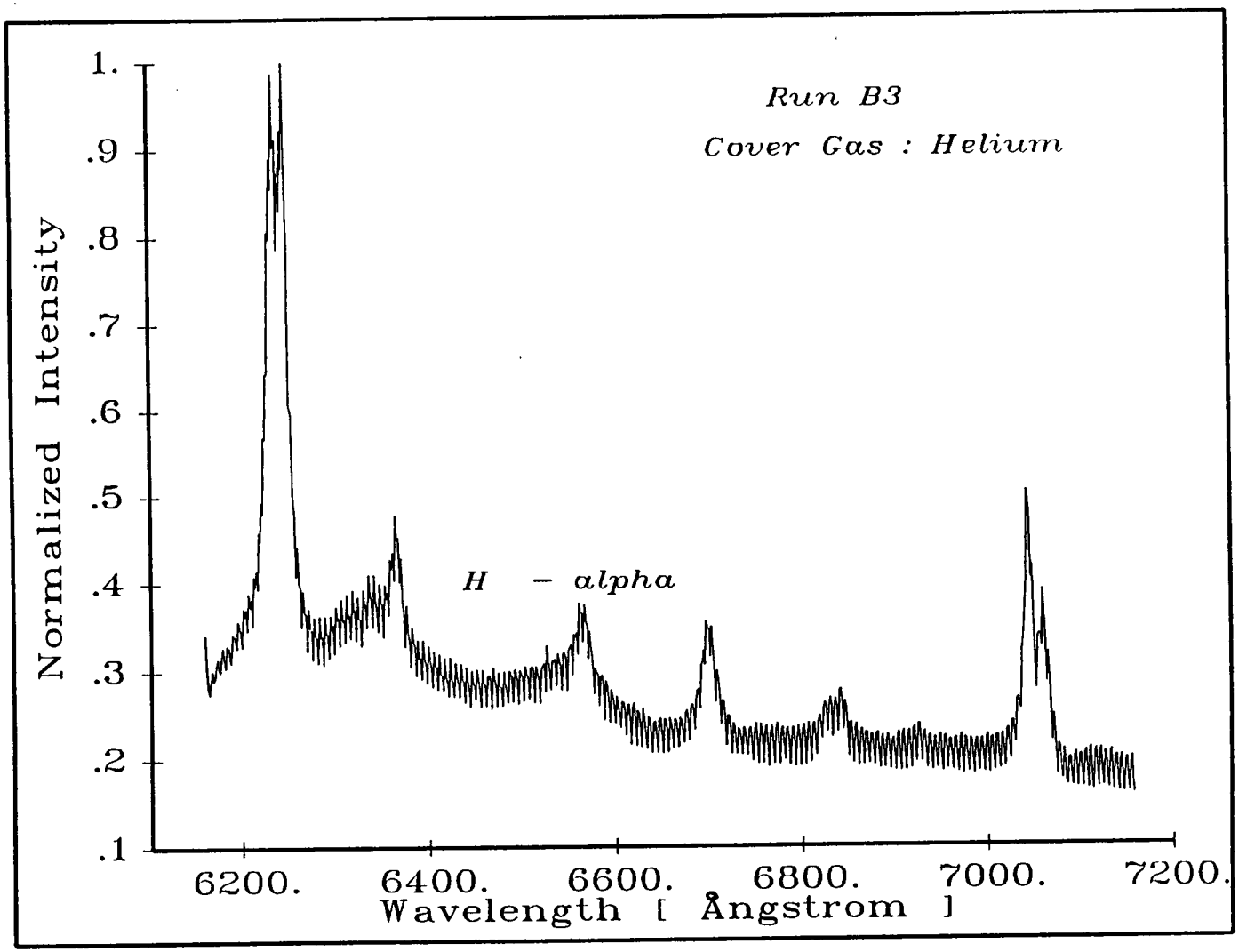


Figure IV-13. Averaged spectrum of plasma with helium.

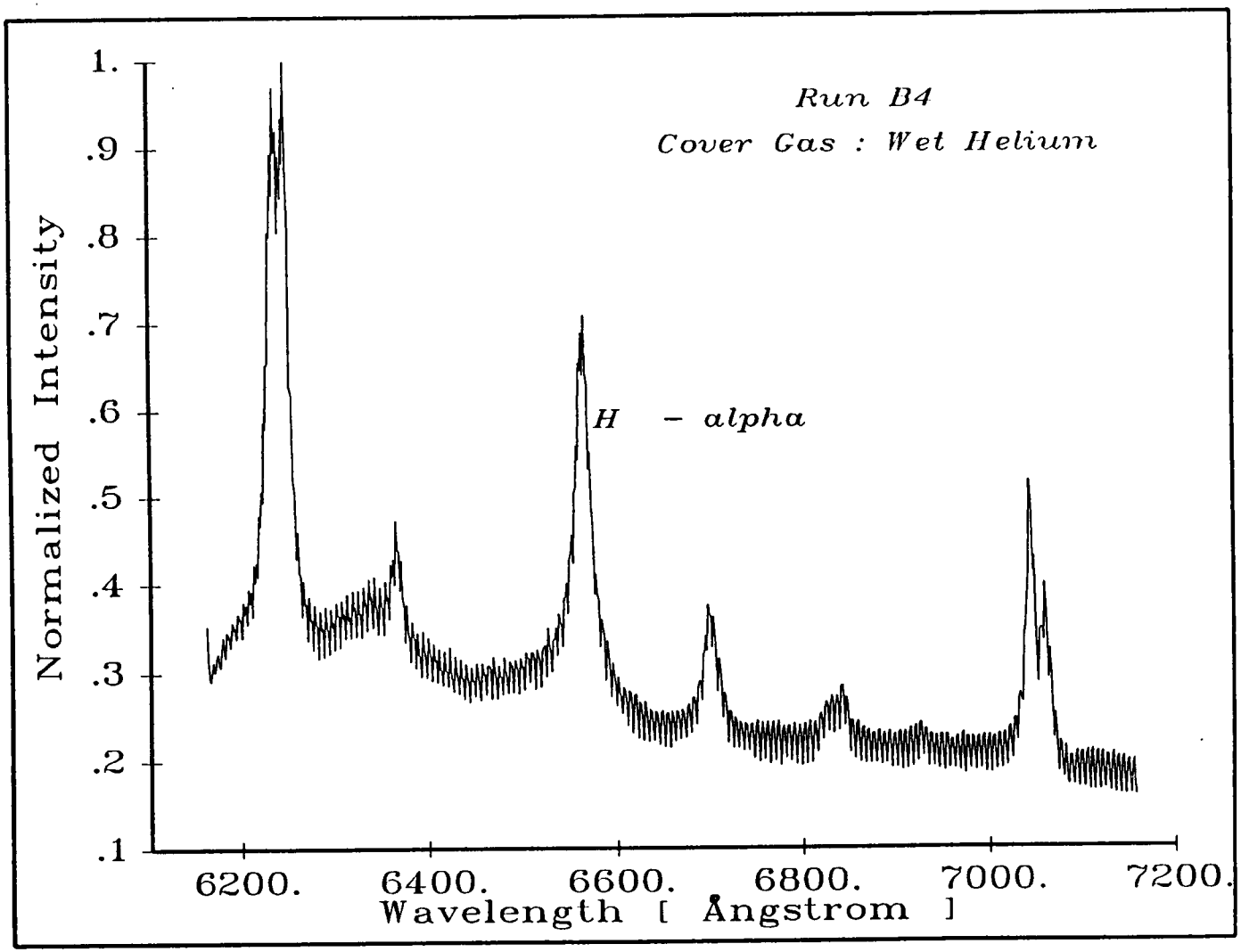


Figure IV-14. Averaged spectrum of plasma with wet helium.

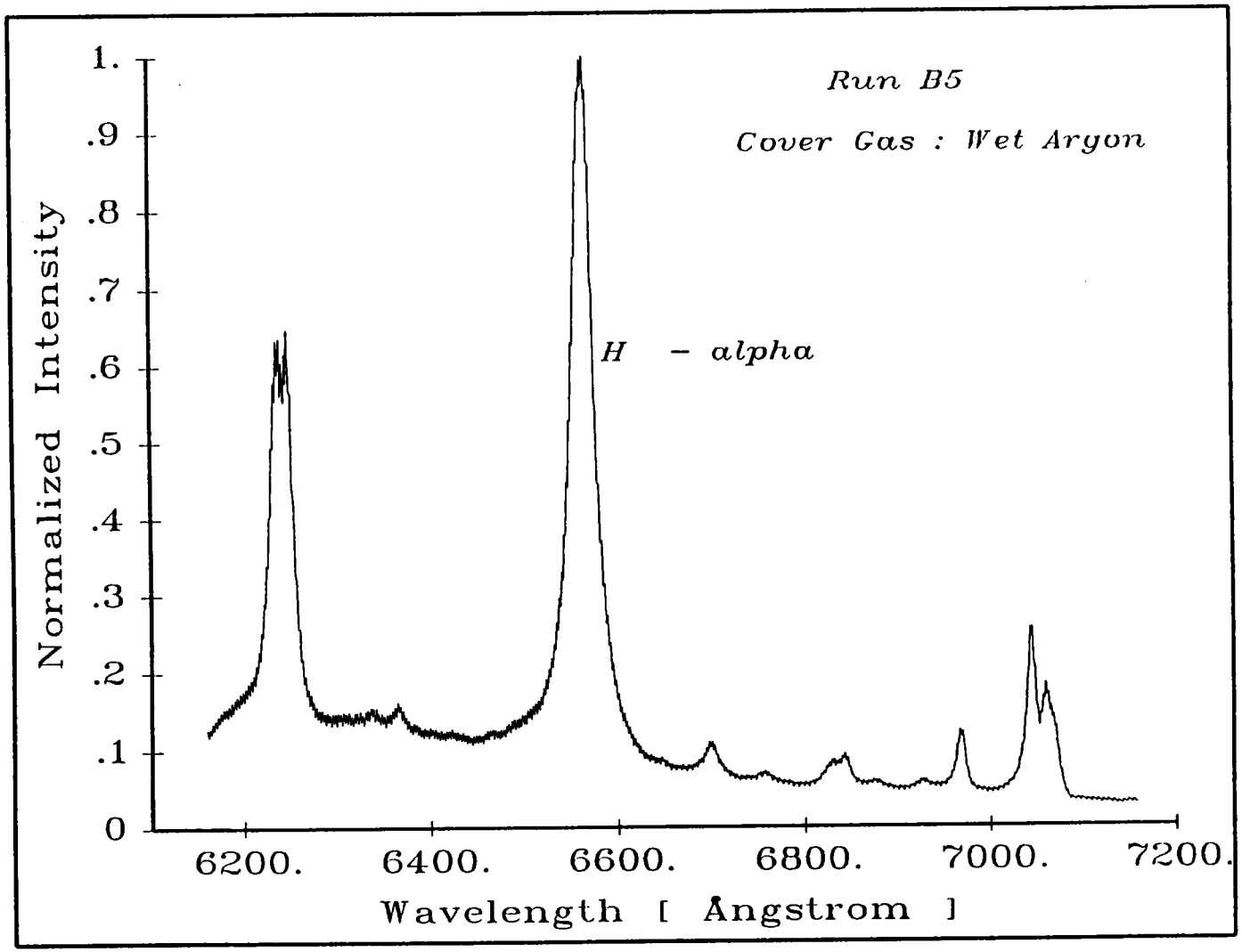


Figure IV-15. Averaged spectrum of plasma with wet argon.

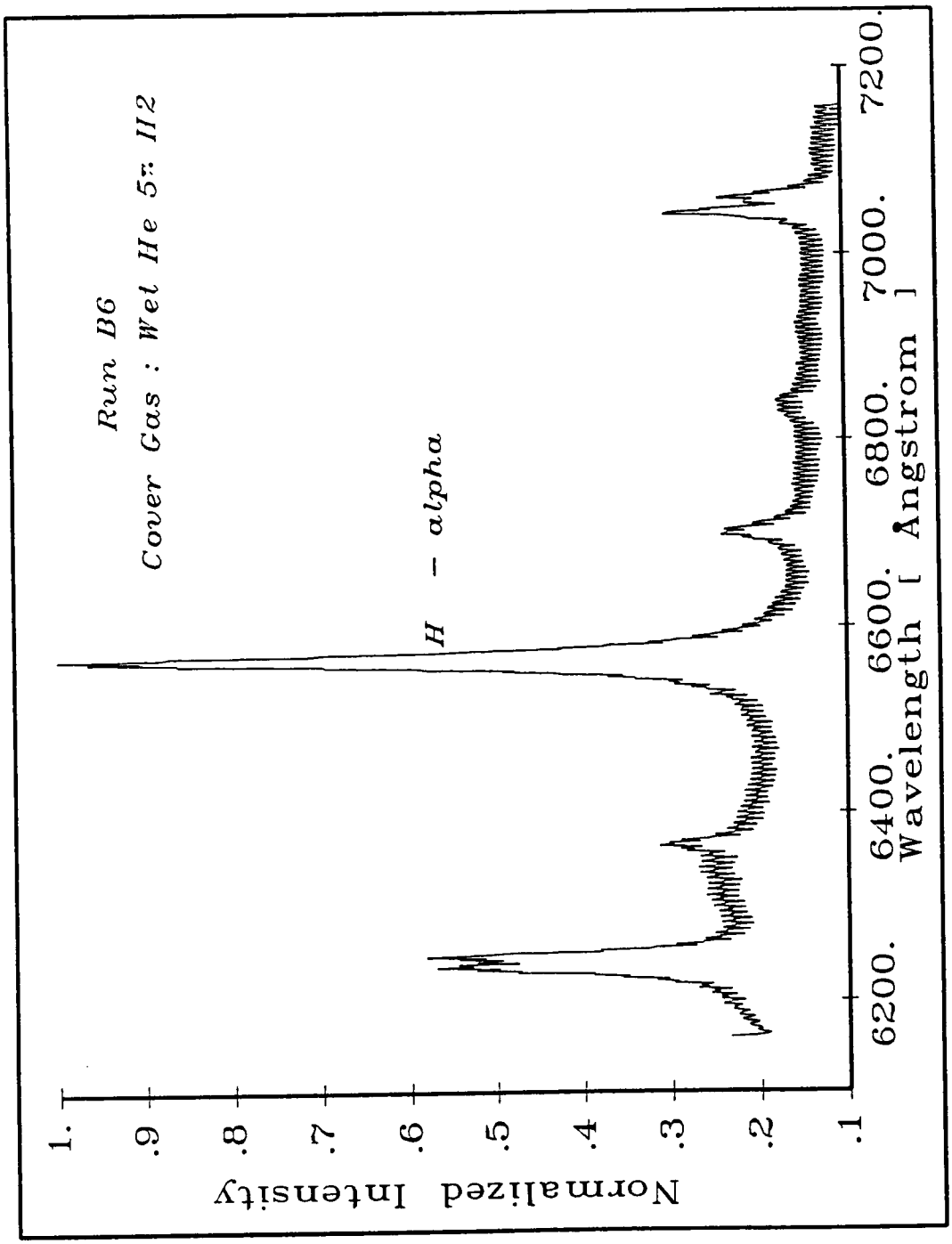


Figure IV-16. Averaged spectrum of plasma with wet He 5% H_2.

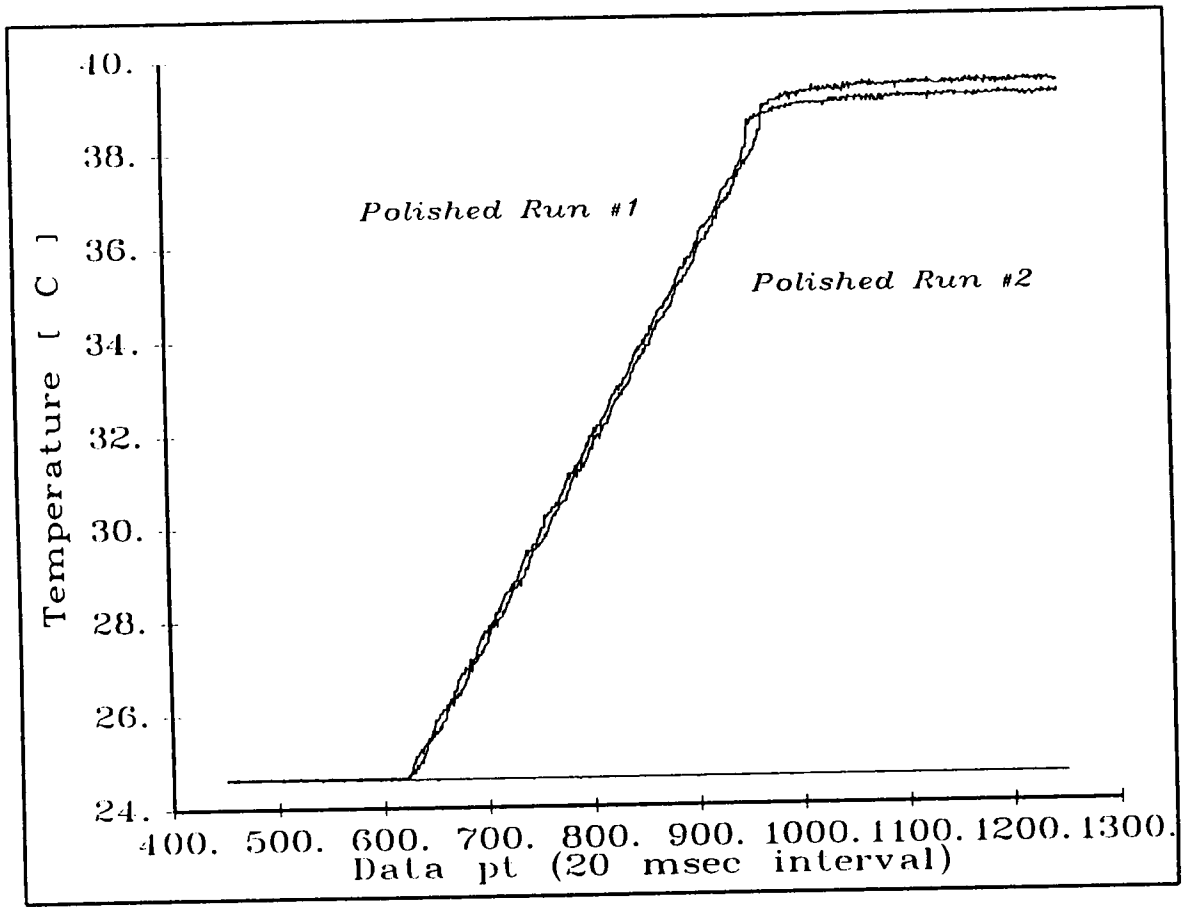


Figure IV-17. Thermal history for surface absorptivity run on polished surface.

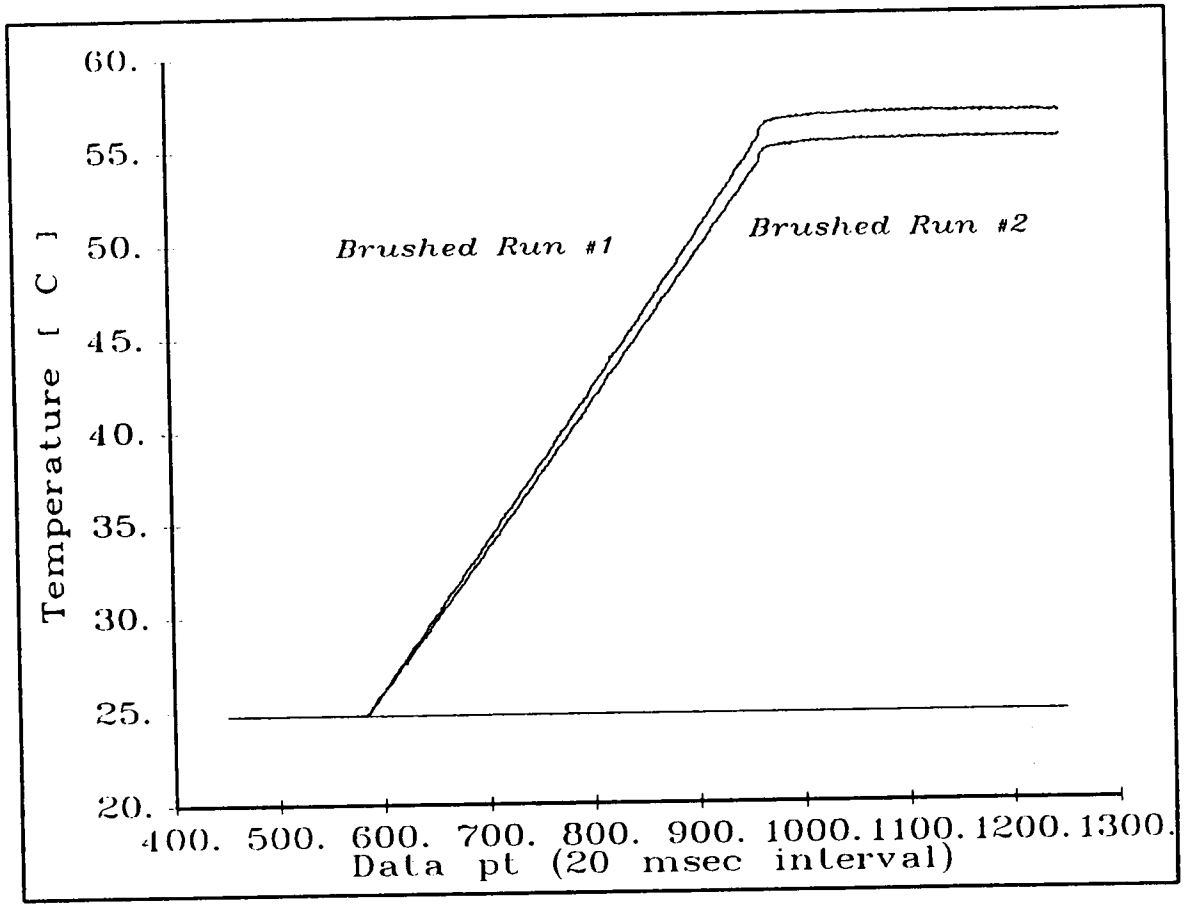


Figure IV-18. Thermal history for surface absorptivity run on brushed surface.

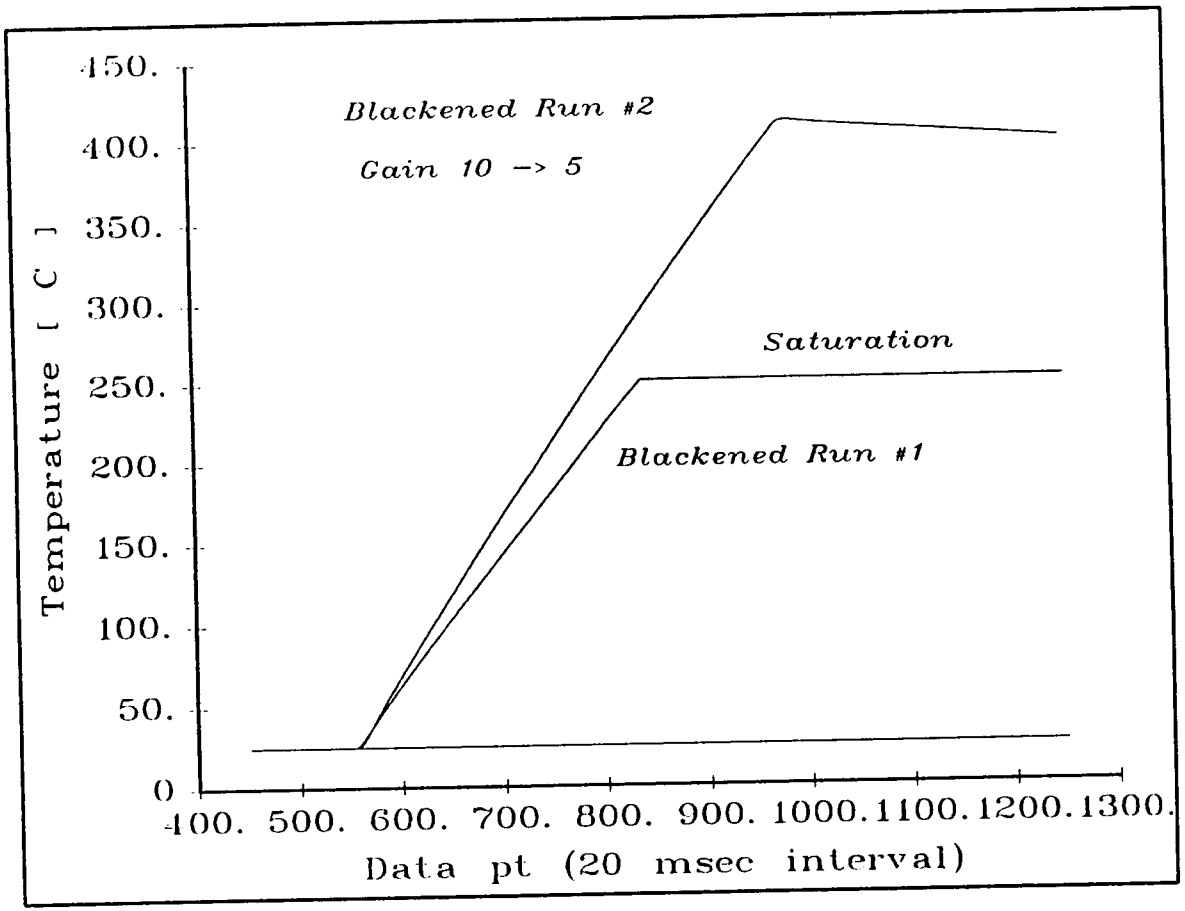


Figure IV-19. Thermal history for surface absorptivity run on blackened surface.

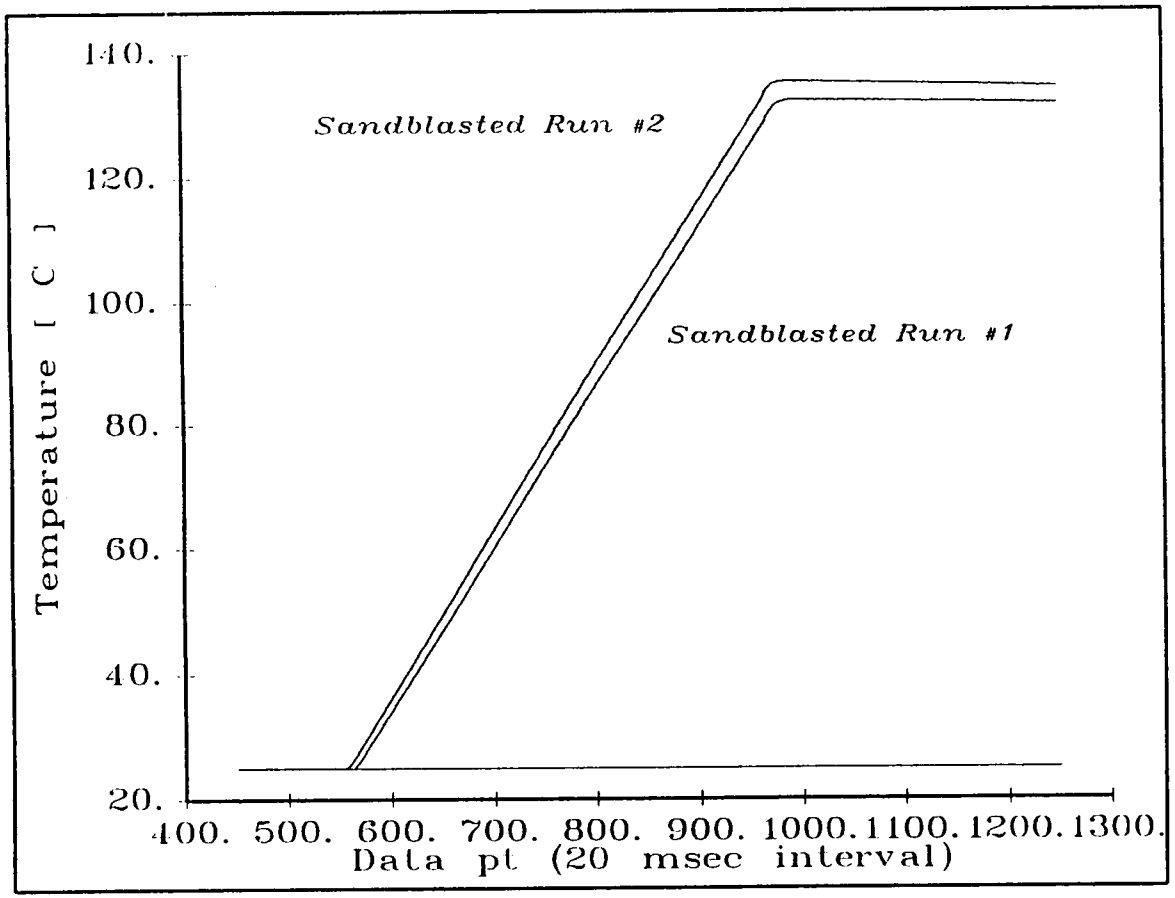


Figure IV-20. Thermal history for surface absorptivity run on sandblasted surface.

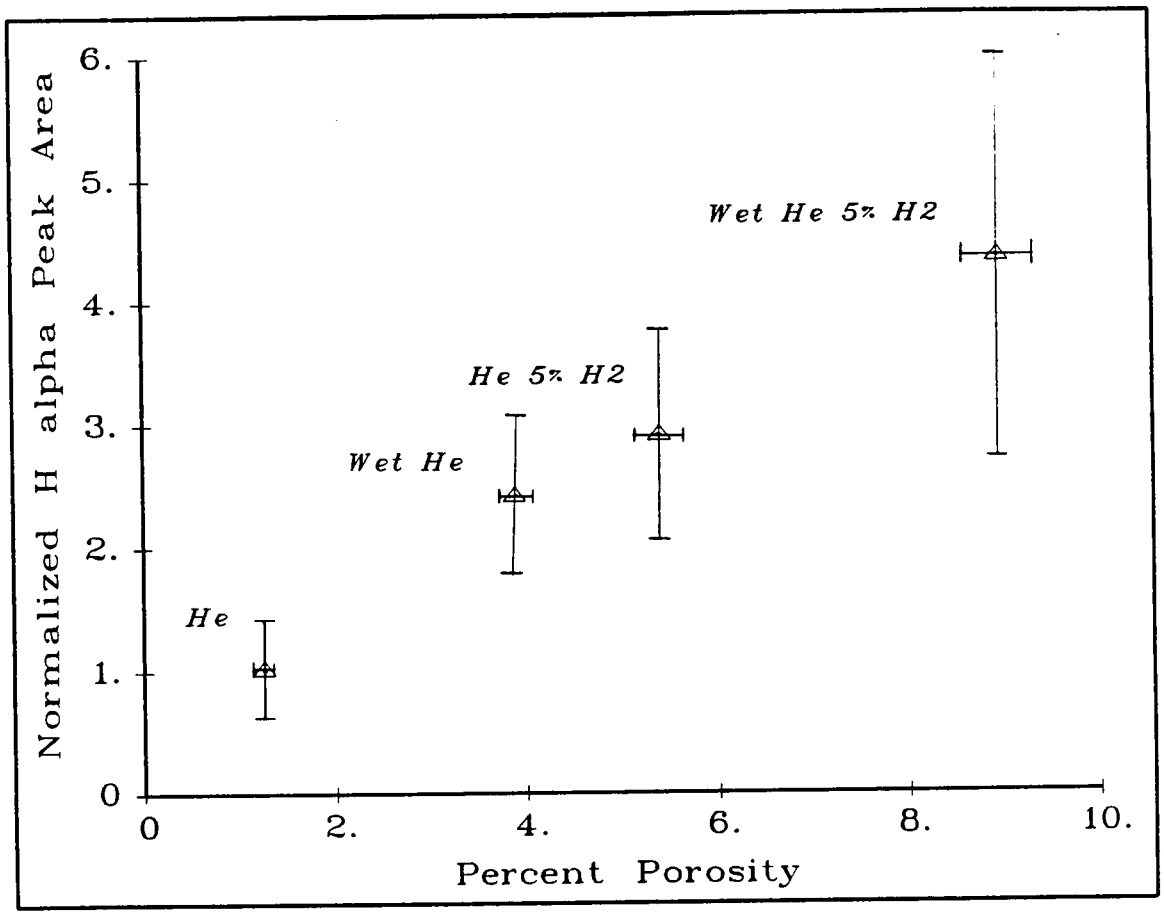


Figure V-1. Plot of normalized area under H_α peak versus percent porosity for helium-based cover gases (Normalized to helium).

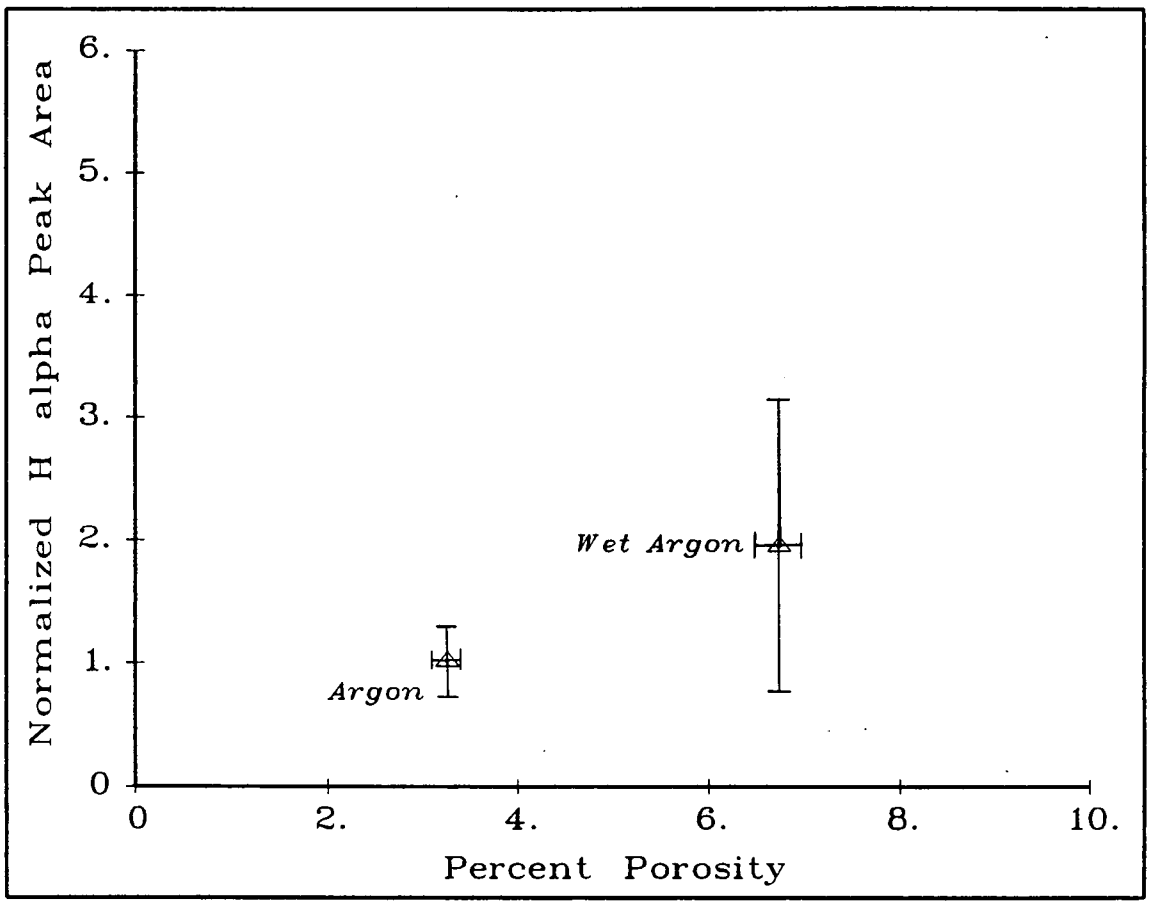


Figure V-2. Plot of normalized area under H_α peak versus percent porosity for argon-based cover gases (Normalized to argon).

VITA

Michael Leon Languell was born in Muncie, Indiana on April 27, 1961. He attended elementary school in Virginia Beach, Virginia; however, his formative years, ages 13 to 17, were spent in Vina del Mar, Chile, South America. He graduated from Kempsville High School of the Virginia Beach School system in June of 1979. The following August he enrolled in the Nuclear Engineering Program at North Carolina State University. While in this program, he was in the Cooperative Education Program working at North Anna Nuclear Power Station for VEPCO. Due to the social and political trends facing the nation, and personal choice, he opted to change his major to that of Materials Engineering in 1982. He received a Bachelor of Science degree in December of 1985.

While attending N.C. State University, he was a member of the varsity fencing team as part of the sabre squad for three years. His hobbies include: water skiing, wind surfing, and gold prospecting.

The author is a member of the Mining, Metallurgical and Materials Society, American Ceramic Society, and American Society of Metals. His career goal is to become involved in the development and transfer of materials related technologies at the international level.